Theory of interactions between cavity photons induced by a mesoscopic circuit

Audrey Cottet[1] and Zaki Leghtas[2,1]
[1] *Laboratoire de Physique de l'Ecole normale supérieure, ENS, Université PSL, CNRS, Sorbonne Université, Université de Paris, F-75005 Paris, France and*
[2] *Centre Automatique et Systèmes, Mines-ParisTech, PSL Research University, 60, bd Saint-Michel, 75006 Paris, France*
(Dated: October 18, 2019)

We use a quantum path integral approach to describe the behavior of a microwave cavity coupled to a dissipative mesoscopic circuit. We integrate out the mesoscopic electronic degrees of freedom to obtain a cavity effective action at fourth order in the light/matter coupling. By studying the structure of this action, we establish conditions in which the cavity dynamics can be considered as Markovian. In this case, one can use a Lindblad equation to describe the cavity quantum dynamics, with effective parameters set by electronic correlation functions. This equation reveals that the mesoscopic circuit induces an effective Kerr interaction and two-photon dissipative processes. We use our method to study the effective dynamics of a cavity coupled to a double quantum dot with normal metal reservoirs. If the cavity is driven at twice its frequency, the double dot circuit generates photonic squeezing and non-classicalities visible in the cavity Wigner function. In particular, we find a counterintuitive situation where mesoscopic dissipation enables the production of photonic Schrödinger cats. These effects can occur for realistic circuit parameters. Our method can be generalized straightforwardly to more complex circuit geometries with, for instance, multiple quantum dots, and other types of fermionic reservoirs such as superconductors and ferromagnets.

PACS numbers: 42.50.Pq, 74.25.N-,73.23.-b, 73.63.Fg

I. INTRODUCTION

Embedding nonlinear Josephson circuits into microwave cavities has enabled impressive progress in the quantum control of microwave light[1]. Indeed, the field of circuit Quantum Electrodynamics (QED) offers many functionalities. For instance, squeezed photonic states, where the uncertainty of one quadrature is reduced below the zero-point level, can be obtained by embedding a nonlinear circuit such as a Superconducting Quantum Interference Device (SQUID) array into a microwave cavity[2]. A classical cavity state can evolve into a quantum superposition of coherent states due to an effective Kerr interaction provided by a superconducting quantum bit[3]. One can also generate arbitrary quantum superpositions of Fock states by using the time-dependent coupling of a superconducting qubit to a microwave resonator[4,5]. For most quantum protocols implemented so far, cavity damping is a spurious effect. However, it has been demonstrated experimentally that in a nonlinear circuit QED setup driven with microwaves, photon-number dependent losses can be used to prepare photonic Schrödinger cat states[6] and stabilize autonomously Fock states[7]. This result contributes to a research field called "reservoir engineering", which promotes the idea that, contrarily to the common belief, dissipation is not always harmful for the quantumness of a system[8–11]. Thanks to this rich phenomenology, nonlinear microwave cavities offer many possibilities of applications, from sensing to quantum information and communication. For example, squeezed states of light offer a powerful resource for quantum-enhanced sensing[12,13]. More recently, quantum computing schemes have been suggested, where quantum information would be encoded in a manifold of cavity states stabilized autonomously by two-photon dissipation[14]. In this context, the photonic Wigner function is a widely measured quantity to characterize the joint statistics of the cavity field quadratures[15]. It is obtained experimentally by performing the cavity tomography[5].

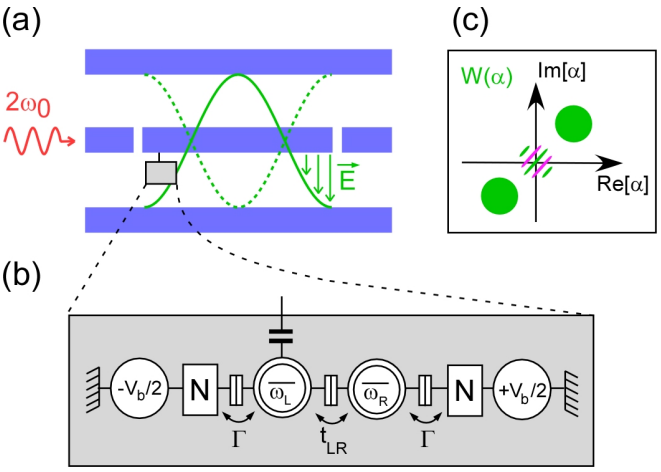

FIG. 1: Example of Mesoscopic QED device. Panel (a): Microwave cavity ac driven at twice the cavity frequency ω_0. The nanocircuit (in grey) is coupled capacitively to the cavity central conductor at an electric field node. Panel (b): Double quantum dot coupled to normal metal reservoirs N with a tunnel rate Γ. The dots are tunnel coupled with a hopping strength t_{LR}. The normal metal reservoirs have a voltage bias V_b. Panel (c): Schematic representation of the cavity Wigner function as a function of the field quadratures, measured by performing the cavity tomography.

In standard Circuit QED experiments, the Joseph-

son circuits coupled to microwave cavities are exclusively made of superconducting metals and Josephson junctions. However, due to the versatility of microwave fabrication techniques, the connection between Circuit QED and mesoscopic physics is naturally growing[16,17]. Recently, circuits enclosing a single[18] or a double[19] quantum dot and normal[18,19], ferromagnetic[20,21] or superconducting reservoirs[22,23] have been coupled to microwave cavities. In the experiments performed so far, microwave cavities have appeared as a powerful means to characterize the electronic spectrum and dynamics of mesoscopic circuits. However, the scope of Mesoscopic QED could go far beyond. Indeed, mesoscopic circuits are intrinsically nonlinear due to their anharmonic energy spectrum. Besides, fermionic reservoirs represent a specific source of dissipation which involves electrically controlled quantum transport. It is therefore appealing to investigate the potentialities of Mesoscopic QED for producing quantum cavity states. In this direction, entangled light/matter states due to a strong charge/photon[23–25] or spin/photon[21,26–28] coupling have been obtained in recent experiments, using double quantum dots circuits. However, many more situations remain to be explored.

On the theory side, the effect of dissipative fermionic reservoirs in Mesoscopic QED setups has been mostly investigated in the semiclassical regime where the number of cavity photons is so large that quantum fluctuations in the photon number can be disregarded[22,29–32]. Otherwise, a sequential tunneling description of quantum transport has been used, which is valid only for very small tunnel rates[33–38]. A general quantum description of Mesoscopic QED is lacking. One needs to develop a theory which describes the cavity quantum dynamics in the presence of dissipative mesoscopic transport. This description must apply to complex circuit configurations with arbitrary tunnel couplings to voltage-biased fermionic reservoirs. It is also important to take into account the nonlinear photonic effects inherited from the light/matter interactions, which have been eluded so far in the theory of Mesoscopic QED, and offer a vast field of investigation. This requires to work beyond the second order treatment of the light/matter coupling.

In this work, we fill these gaps by employing a quantum path integral technique along the Keldysh contour, which is particularly convenient to integrate out electronic degrees of freedom and obtain an effective description of the cavity nonlinear behavior[39]. We consider a cavity with frequency ω_0 coupled to a mesoscopic circuit and excited with a microwave tone at frequency $2\omega_0$ with a moderate amplitude ε_p (i.e. ε_p can be treated to first order). We note g the order of magnitude of the light/matter coupling in the mesoscopic QED device. We obtain the effective quantum action of the cavity to fourth order in g/ω_0. This action depends on electronic correlation functions of the mesoscopic circuit, which we express in terms of Keldysh Green's functions. It reveals that, in the general case, the cavity has a non-Markovian dynamics and is subject to photon-photon interactions mediated by the mesoscopic circuit. However, we establish sufficient conditions on the mesoscopic correlators for having a Markovian cavity dynamics. In this case, the $2\omega_0$ drive produces a coherent two-photon drive and an unusual squeezing dissipation at third order in g/ω_0. Additionally, the mesoscopic circuit induces, at fourth order in g/ω_0, Kerr photon-photon interaction as well as stochastic two-photon losses and gains. Importantly, our results are valid for tunnel couplings rates to the reservoirs of the mesoscopic circuit smaller as well as larger than the electronic temperature since no sequential tunneling hypothesis is required. We make the realistic assumption that the cavity has a large quality factor and a dressed linewidth much smaller than the mesoscopic resonances linewidth. We finally disregard Coulomb interactions in the mesoscopic circuit.

We use our method to study the quantum dynamics of a microwave cavity coupled to a non-interacting double quantum dot (DQD) with normal metal contacts biased with a voltage V_b. We identify two situations where the effective dynamics of the cavity is Markovian but nevertheless displays clear non-linear light/matter interaction effects. The first situation is the limit of a low light/matter coupling ($g \sim 0.01\omega_0$). In this case, we derive an effective Lindblad equation description of the cavity behavior to third order in g/ω_0, from which we obtain an analytic expression of the cavity Wigner function in stationary conditions. The $2\omega_0$ drive produces a coherent injection/withdrawal of photon pairs in the cavity and an unusual squeezing dissipative process. This leads to a squeezing of the cavity vacuum, which depends non trivially on the system parameters. The second Markovian situation is when the double dot is resonant with $2\omega_0$ and has moderate interdot hopping and tunnel couplings to its reservoirs, and the light/matter coupling is moderate ($g \sim 0.1\omega_0$). In this case, a Lindblad equation to fourth order in g/ω_0 is necessary to describe the cavity dynamics. In this limit, we find that, in the absence of a cavity drive ($\varepsilon_p = 0$), dissipative transport in the double dot circuit can enable the stochastic absorption and/or emission of photon pairs in the cavity, depending on the value of V_b. When the cavity is ac driven ($\varepsilon_p \neq 0$) with $V_b = 0$, we show, with numerical simulations of the photonic Lindblad equation, that the DQD circuit can be used to produce photonic Schrödinger cat states. This effect is expected for realistic circuit parameters. It is due to a combination of the two photon drive in $\varepsilon_p g^3/\omega_0^3$ and the photon pair damping in g^4/ω_0^3. Hence, counterintuitively, mesoscopic dissipation enables the generation of a quantum superposition of cavity states. More generally, our work demonstrates the interest of Mesoscopic QED for the preparation of quantum photonic states.

Our approach can be used to explore many more circuit geometries and protocols, with single or multiple quantum dots, or extended nanoconductors modeled with the Hubbard model[30,32,40–42], and different types of fermionic reservoirs. Hence, it should be instrumental for the development of Mesoscopic QED in the nonlinear quantum

regime, towards which experimental efforts are headed.

This article is organized as follows. Section II introduces the Mesoscopic QED Hamiltonian and discusses a direct density matrix description of Mesoscopic QED and its drawbacks. Section III presents the general description of Mesoscopic QED with the path integral approach. It also explains how the cavity effective action leads to a Markovian Lindblad description, at third order in g/ω_0 for any parameters, or at fourth order in g/ω_0 provided some mesoscopic correlation functions fulfill a Markovian condition. Section IV applies the results of section III to the example of a microwave cavity coupled to a double quantum dot. In particular, it shows how the double dot can be used to squeeze the cavity vacuum or to produce photonic Schrödinger cats. In section V, we discuss the perspectives of generalization of our approach to a large span of mesoscopic circuits. Appendix A gives details on the derivation of the cavity effective action at fourth order in g/ω_0. Appendix B1 gives a direct calculation of the possible semiclassical values of the cavity photonic amplitude at fourth order in g/ω_0 (without using the path integral approach). This enables a semiclassical interpretation of some of the parameters which occur in the cavity effective action. Appendix B2 shows an alternative way to determine the possible values of the cavity photonic amplitude, by considering the saddle points of the cavity action. The agreement between the results of Appendix B1 and Appendix B2 at fourth order in g/ω_0 provides an important sanity check for our approach. Appendix D establishes a quantitative equivalence at order 2 in g/ω_0 between the Lindblad equation arising from the direct density matrix approach and the Lindblad equation arising from the path integral approach. Appendix E gives details on the calculation of the cavity Wigner function. Appendix F gives details on the dependence of the photonic squeezing effect on the double dot parameters.

II. DESCRIPTION OF MESOSCOPIC QED WITH A DIRECT DENSITY MATRIX APPROACH

A. System Hamiltonian

We consider a cavity with bare frequency ω_0 excited by a microwave drive $\varepsilon_{ac}(t)$, and coupled to a mesoscopic circuit. This circuit contains N discrete orbitals with index d, coupled to fermionic reservoirs with a continuum of states with index k. The mesoscopic circuit can be for instance a quantum dot circuit, in which case the orbitals d are located in the dots[17–19]. Each orbital d is coupled to the electric quadrature of the cavity field with a constant g_d (see Ref.[43] for a first-principles description of this effect and a microscopic expression of g_d). The resulting Mesoscopic QED device can be described with the Hamiltonian

$$\begin{aligned}\hat{H}_{tot} &= \omega_0 \hat{a}^\dagger \hat{a} + \varepsilon_{ac}(t)\left(\hat{a}^\dagger + \hat{a}\right) + \hat{h}_b \\ &+ \hat{H}_{meso} + \sum_d g_d (\hat{a}^\dagger + \hat{a}) \hat{c}_d^\dagger \hat{c}_d\end{aligned} \tag{1}$$

with

$$\begin{aligned}\hat{H}_{meso} &= \sum_d \omega_d \hat{c}_d^\dagger \hat{c}_d + \sum_{d<d'} \left(t_{d',d} \hat{c}_{d'}^\dagger \hat{c}_d + H.c. \right) \\ &+ \sum_{k,d} \left(t_{k,d} \hat{c}_k^\dagger \hat{c}_d + H.c. \right) + \sum_k \omega_k \hat{c}_k^\dagger \hat{c}_k\end{aligned} \tag{2}$$

Above, $\hat{a}^\dagger$ is the cavity photon creation operator, $\hat{c}_d^\dagger$ the electron creation operator in the discrete orbital $d \in [1, N]$ and $\hat{c}_k^\dagger$ an electron creation operator in a level k of one of the fermionic reservoirs. In the general case, the indices k and d include the spin degree of freedom. We do not specify the exact Mesoscopic circuit geometry for the moment because our approach is general. The tunnel hopping strength between two orbitals d and $d'[k]$ located in neighboring sites of the circuit is noted $t_{d'[k],d}$. We use $\hbar = 1$. Intrinsic cavity damping is described by the Hamiltonian $\hat{h}_b$ which we do not specify here. In most cases, the orbital energy ω_d of site d can be finely tuned with an electrostatic gate, and bias voltages can be applied to the fermionic reservoirs to induce electronic transport. In the following, we assume that an ac drive

$$\varepsilon_{ac}(t) = (\varepsilon_p e^{-i2\omega_0 t} + \varepsilon_p^* e^{i2\omega_0 t})/2 \tag{3}$$

is applied to the cavity. We will see that both components in $e^{-i2\omega_0 t}$ and $e^{i2\omega_0 t}$ contribute to the the cavity response through higher order processes (effect in $(g/\omega_0)^3$ at least). For simplicity, we do not describe explicitly the microwave inputs and outputs of the cavity but this can be added straightforwardly by using the input/output theory[29,44,45].

B. Direct density matrix approach and its drawbacks

The most commonly used description of Circuit QED is the density matrix approach which consists in expressing directly the time evolution of the system density matrix. Here we will shortly discuss this approach to point out its weaknesses and the interest of the path integral approach in the context of nonlinear Mesoscopic QED.

We assume that the interaction term $\hat{V}$ is a perturbation in the system Hamiltonian, in comparison with the cavity contribution in ω_0 and mesoscopic contribution $\hat{H}_{meso}$. For simplicity, in this section, we also assume that there is no cavity drive ($\varepsilon_p = 0$) and no cavity intrinsic dissipation (i.e. $\hat{h}_b$ is negligible). In these conditions, it is convenient to use the interaction picture, where the density matrix $\rho^I(t) = e^{i\omega_0 \hat{a}^\dagger \hat{a} t + i\hat{H}_{meso} t} \rho(t) e^{-i\omega_0 \hat{a}^\dagger \hat{a} t - i\hat{H}_{meso} t}$ of the full mesoscopic QED device (cavity+mesoscopic circuit) has an

evolution equation

$$\frac{\partial \rho^I(t)}{\partial t} = -i[\hat{V}(t), \rho^I(t)] \tag{4}$$

with

$$\hat{V}(t) = \hat{N}(t)\left(\hat{a}e^{-i\omega_0 t} + \hat{a}^\dagger e^{i\omega_0 t}\right) \tag{5}$$

$$\hat{N}(t) = \sum_d g_d \hat{n}_d(t) \tag{6}$$

and

$$\hat{n}_d(t) = e^{i\hat{H}_{meso}t}\hat{c}_d^\dagger \hat{c}_d e^{-i\hat{H}_{meso}t} \tag{7}$$

Note that $\hat{H}_{meso}$ and $\hat{c}_d^\dagger \hat{c}_d$ do not commute due to dot-dot and dot-reservoir tunneling. Hence, from Eqs. (6) and (7), $\hat{N}(t)$ depends on time.

We now discuss the expression of the cavity dynamics at second order in g. The integration of Eq.(4) gives

$$\rho^I(t) = \rho^I(t_0) - i\int_{t_0}^{t} dt_1 [V(t_1), \rho^I(t_1)] \tag{8}$$

with t_0 a reference time far in the past. Inserting this equation back in Eq.(4) gives

$$\frac{\partial \rho^I(t)}{\partial t} = -i[\hat{V}(t), \rho^I(t_0)] - \int_{t_0}^{t} dt_1 [\hat{V}(t), [V(t_1), \rho^I(t_1)]] \tag{9}$$

In the limit where the mesoscopic system has a correlation time τ which is much shorter than the cavity characteristic timescale of evolution T, only the times t_1 such that $t - t_1 \lesssim \tau$ will contribute in the above integral[46]. Accordingly, one can assume that the mesoscopic system is constantly at equilibrium, i.e.

$$\rho^I(t_1) = \rho^0_{meso} \otimes \rho^I_{cav}(t_1) \tag{10}$$

with ρ^0_{meso} the equilibrium density matrix of the mesoscopic circuit for $g_d = 0$. Finally, since $\tau \ll T$, one can use $\rho^I(t_1) = \rho^0_{meso} \otimes \rho^I_{cav}(t)$ in the above integral, Performing the trace $\underset{k,d}{\mathrm{Tr}}$ on the mesoscopic degrees of freedom, one finally gets

$$\begin{aligned}
&\frac{\partial \rho^I_{cav}(t)}{\partial t} \\
&= -i \underset{k,d}{\mathrm{Tr}}\left[[V(t), \rho^0_{meso} \otimes \rho^I_{cav}(t_0)]\right] \\
&- \int_{t_0}^{t} dt_1 \ \underset{k,d}{\mathrm{Tr}}\left[[V(t), [V(t_1), \rho^0_{meso} \otimes \rho^I_{cav}(t)]]\right]
\end{aligned} \tag{11}$$

A reorganization of Eq.(11) gives, keeping only resonant terms and considering a stationary situation,

$$\begin{aligned}
\frac{\partial \rho^I_{cav}(t)}{\partial t} &= -2\,\mathrm{Im}[\chi_B(\omega_0)]\mathcal{L}_{\hat{a}}(\rho^I_{cav}(t)) \\
&- 2\,\mathrm{Im}[\chi_A(\omega_0)]\mathcal{L}_{\hat{a}^\dagger}(\rho^I_{cav}(t)) \\
&- i\,\mathrm{Re}[\chi_B(\omega_0) - \chi_A(\omega_0)]\ [\hat{a}^\dagger \hat{a}, \rho^I_{cav}(t)] + o(\check{g}^2)
\end{aligned} \tag{12}$$

Above,

$$\mathcal{L}_{\hat{L}_j}(\rho^I_{cav}) = \sum_j \left(\hat{L}_j \rho^I_{cav} \hat{L}_j^\dagger - \frac{1}{2}\{\hat{L}_j^\dagger \hat{L}_j, \rho^I_{cav}\}\right) \tag{13}$$

is the Lindblad superoperator associated to the jump operator $\hat{L}_j$. We have disregarded the first order term in $\check{g}/\omega_0$ which is non-resonant with the cavity. The mesoscopic correlators

$$\chi_A(t) = -i\theta(t)\left\langle \hat{N}(0)\hat{N}(t)\right\rangle \tag{14}$$

and

$$\chi_B(t) = -i\theta(t)\left\langle \hat{N}(t)\hat{N}(0)\right\rangle \tag{15}$$

whose Fourier transforms $\chi_{A[B]}(\omega) = \int dt\ \chi_{A[B]}(t)e^{i\omega t}$ appear in Eq.(12), have to be evaluated to second order in the light/matter interaction. More precisely, from Eq.(6), one can use $\left\langle \hat{N}(t')\hat{N}(t)\right\rangle = \sum_{d,d'} g_d g_{d'} A_{d',d}(t',t)$ and $A_{d',d}(t',t) = \left\langle \hat{c}^\dagger_{d'}(t')\hat{c}_{d'}(t')\hat{c}^\dagger_d(t)\hat{c}_d(t)\right\rangle_0$ where $\langle\rangle_0$ denotes a statistical average calculated for $g_d = 0$ for any d, i.e. $A_{d',d}(t',t) = \mathrm{Tr}\left[\rho^0_{meso}\hat{c}^\dagger_{d'}(t')\hat{c}_{d'}(t')\hat{c}^\dagger_d(t)\hat{c}_d(t)\right]$. In the absence of Coulomb interactions, the evaluation of $A_{d,d'}$ can be done straightforwardly by using the Wick theorem (see for instance Ref.[47]).

To describe the dynamics of ρ^I_{cav} beyond the second order in g, one straightforward idea is to iterate Eq.(8). This gives

$$\begin{aligned}
&\frac{\partial \rho^I_{cav}(t)}{\partial t} \\
&= -i\underset{k,d}{\mathrm{Tr}}\left[[V(t), \rho^I(t_0)]\right] - \int_{t_0}^{t} dt_1 \ \underset{k,d}{\mathrm{Tr}}\left[[V(t), [V(t_1), \rho^I(t_0)]]\right] \\
&+ i\iint_{t_0,t_0}^{t,t_1} dt_2 dt_3 \ \underset{k,d}{\mathrm{Tr}}\left[[V(t), [V(t_1), [V(t_2), \rho^I(t_0)]]]\right] \\
&+ \iiint_{t_0,t_0,t_0}^{t,t_1,t_2} dt_1 dt_2 dt_3 \ \underset{k,d}{\mathrm{Tr}}[[V(t), [V(t_2), [V(t_3), [V(t_4), \rho^I(t_0)]]]]] \\
&+ o(\check{g}^4)
\end{aligned} \tag{16}$$

At this stage, conceptual difficulties as well as calculation heaviness make the generalization of Eq.(12) nontrivial. First, a back-action of the cavity on the mesoscopic density matrix should be taken into account. This means that expression (10) cannot be used to express $\rho^I(t_0)$ in Eq.(16). Hence, it will be more difficult to introduce independently defined mesoscopic correlators in the expression of $\partial\rho^I_{cav}(t)/\partial t$. Besides, the dynamics of the system is not anymore Markovian in the general case, so that $\rho^I_{cav}(t)$ does not appear naturally in the right member of Eq.(16). Finally, even in a case where a generalization of the Markovian Eq.(12) would be possible, due to the iterative structure of Eq.(16), the number of

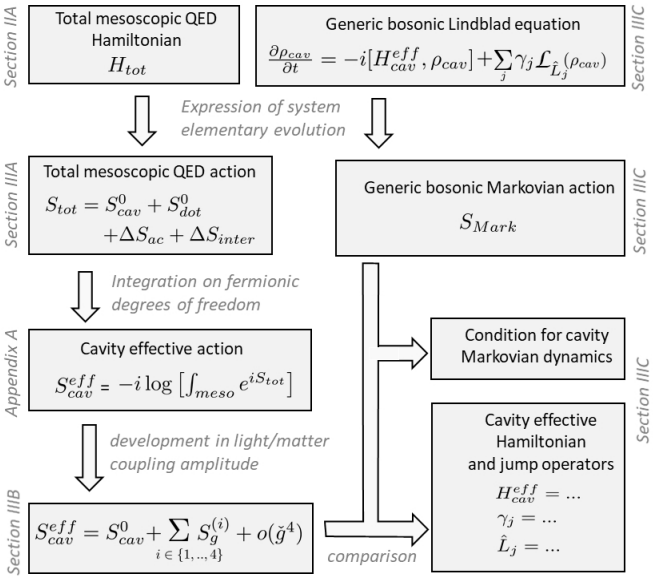

FIG. 2: Synoptic table of the theoretical approach introduced in section III

mesoscopic correlators to define would explode, and the explicit calculation of these correlators from the mesoscopic circuit Hamitonian would be a lengthy task. In fact, all these difficulties stem from the fact that the trace on the mesoscopic degrees of freedom is performed after the time evolution of $\rho^I(t)$ is expressed. It is thus crucial to use a calculation method where the electronic degrees of freedom are integrated earlier, i.e. at the level of the device Hamiltonian. This is why we will develop an efficient quantum path integral description of Mesoscopic QED in the next section.

III. GENERAL DESCRIPTION OF MESOSCOPIC QED WITH THE QUANTUM PATH INTEGRAL FORMALISM

This section describes a general method based on the quantum path integral description to describe the effective behavior of a microwave cavity coupled to a mesoscopic circuit. From the Mesoscopic QED Hamiltonian of Eq.(1), we express the global quantum action of the system (see section III A). The fermionic degrees of freedom in this action can be integrated out to obtain the cavity effective action (see section III B). We compare this action to the action given by a generic Lindblad description of a cavity dynamics (see section III C). This enables us to establish a criterion to have a cavity Markovian dynamics at fourth order in the light/matter coupling. When this criterion is fulfilled, we can finally write the cavity effective Lindblad equation. This approach is summarized in the synoptic table of Figure 2.

A. Quantum action of the whole Mesoscopic QED device

A generic description of Mesoscopic QED can be built by expressing the Schwinger-Keldysh partition function of the system with a quantum path integral along the Keldysh contour[39]. To this end, we define, along the forward and backward branches of the Keldysh contour, the fields $\varphi_\pm(t)$, $\bar{\varphi}_\pm(t)$, $\psi_{\pm,d}(t)$ and $\bar{\psi}_{\pm,d}(t)$, which correspond to a possible "realization" of the operators $\hat{a}$, $\hat{a}^\dagger$, $\hat{c}_d$ and $\hat{c}^\dagger_d$ over time[48]. It is convenient to define the average and relative field components $\varphi_{cl/q}(t) = (\varphi_+(t) \pm \varphi_-(t))/\sqrt{2}$, $\bar{\varphi}_{cl/q}(t) = (\bar{\varphi}_+(t) \pm \bar{\varphi}_-(t))/\sqrt{2}$, $\psi_{0/1,d}(t) = (\psi_{+,d}(t) \pm \psi_{-,d}(t))/\sqrt{2}$, and $\bar{\psi}_{0/1,d}(t) = (\bar{\psi}_{+,d}(t) \mp \bar{\psi}_{-,d}(t))/\sqrt{2}$. These quantities can be grouped into vectorial fields $\varphi(t) = {}^t\{\varphi_{cl}(t), \varphi_q(t)\}$, $\bar{\varphi}(t) = \{\bar{\varphi}_{cl}(t), \bar{\varphi}_q(t)\}$, $\psi(t) = {}^t\{\psi_0(t), \psi_1(t)\}$ and $\bar{\psi}(t) = \{\bar{\psi}_0(t), \bar{\psi}_1(t)\}$. Note that in the case of a mesoscopic circuit with several discrete orbitals, the fields $\psi_0(t)$ and $\psi_1(t)$ have an orbital structure $\psi_m(t) = {}^t\{\psi_{m,d_1}(t), ..., \psi_{m,d_N}(t)\}$ with $m \in \{0/1\}$. In the main text of this article, all the fields have a time argument t, which is omitted for brevity, except when two times t and t' are involved in an equation. The global Schwinger-Keldysh partition function Z of the mesoscopic QED device and the corresponding quantum action S_{tot} can be obtained directly from Hamiltonian (1) by considering the elementary evolution of the system along the Keldysh contour[39]. This gives

$$Z = \int d[\bar{\varphi}, \varphi, \bar{\psi}, \psi] e^{iS_{tot}(\bar{\varphi}, \varphi, \bar{\psi}, \psi)} \tag{17}$$

with

$$\begin{aligned} S_{tot}(\bar{\varphi}, \varphi, \bar{\psi}, \psi) = S^0_{cav}(\bar{\varphi}, \varphi) + S^0_{meso}(\bar{\psi}, \psi) \\ + \Delta S_{ac}(\bar{\varphi}, \varphi) + \Delta S_{inter}(\bar{\varphi}, \varphi, \bar{\psi}, \psi) \end{aligned} \tag{18}$$

Above, $d[\bar{\varphi}, \varphi, \bar{\psi}, \psi]$ is the differential element associated to the fields $\bar{\varphi}, \varphi, \bar{\psi}$ and ψ. The term

$$S^0_{cav}(\bar{\varphi}, \varphi) = \int_t \begin{bmatrix} \bar{\varphi}_{cl} & \bar{\varphi}_q \end{bmatrix} \begin{bmatrix} 0 & D_t - \frac{i\Lambda_0}{2} \\ D_t + \frac{i\Lambda_0}{2} & i\Lambda_0(1+2n_B) \end{bmatrix} \begin{bmatrix} \varphi_{cl} \\ \varphi_q \end{bmatrix} \tag{19}$$

is the bare cavity action, with $D_t = i\partial t - \omega_0$, $n_B = 1/(e^{\omega_0/k_B T} - 1)$ and Λ_0 a damping rate due to the cavity bath treated in the Markovian approximation[49]. For compactness, we note $\int_{-\infty}^{+\infty} dt = \int_t$. The cavity drive brings a contribution:

$$\Delta S_{ac}(\bar{\varphi}, \varphi) = -\sqrt{2} \int_t (\bar{\varphi}_q + \varphi_q)\, \varepsilon_{ac}(t) \tag{20}$$

The bare action from the mesoscopic circuit is

$$S^0_{meso}(\bar{\psi}, \psi) = \int_{t,t'} \bar{\psi}(t) \check{G}^{-1}(t, t') \psi(t') \tag{21}$$

with $\check{G}$ the mesoscopic circuit Green's function in the absence of light/matter coupling. The contribution from the light/matter coupling is

$$\Delta S_{inter}(\bar{\varphi},\varphi,\bar{\psi},\psi) = -\int\limits_{t,t'} \bar{\psi}(t)(\check{v}(\bar{\varphi},\varphi,t)\delta(t-t'))\psi(t') \tag{22}$$

with $\iint_{-\infty}^{+\infty} dt\ dt' = \int_{t,t'}$ and $\check{v}$ a light/matter coupling function. Both $\check{G}$ and $\check{v}$ are defined below.

The unperturbed mesoscopic circuit Green's function which appears in Eq.(21) has the structure $\check{G}(t,t') = \int\limits_{\omega} \check{G}(\omega)e^{i\omega(t'-t)}$ with[39]

$$\check{G}(\omega) = \begin{bmatrix} \tilde{G}_r(\omega) & \tilde{G}_K(\omega) \\ \tilde{0} & \tilde{G}_a(\omega) \end{bmatrix} \tag{23}$$

the 2×2 mesoscopic Keldysh space. Above, $\tilde{0}$ is a matrix full of zeros in the $N\times N$ the mesoscopic orbitals space. The retarded, advanced and Keldysh components $\tilde{G}_{r/a/K}(\omega)$ of $\check{G}$ also have a $N\times N$ structure in the mesoscopic orbitals space. In the absence of superconducting correlations in a circuit, the elements of $\tilde{G}_r$, $\tilde{G}_a$ and $\tilde{G}_K$ in the line d and column d' can be defined as

$$G_r^{d,d'}(t) = -i\theta(t)\left\langle \{\hat{c}_d(t), \hat{c}_{d'}^\dagger(t=0)\}\right\rangle \tag{24}$$

$$G_a^{d,d'}(t) = i\theta(-t)\left\langle \{\hat{c}_d(t), \hat{c}_{d'}^\dagger(t=0)\}\right\rangle \tag{25}$$

and

$$G_K^{d,d'}(t) = -i\left\langle [\hat{c}_d(t), \hat{c}_{d'}^\dagger(t=0)]\right\rangle \tag{26}$$

respectively, with the Fourier transforms $\tilde{G}_{r/a/K}(\omega) = \int_{-\infty}^{+\infty} dt\ \tilde{G}_{r/a/K}(t)e^{i\omega t}$. At this stage, we do not give a more explicit expression for $\check{G}$ because we consider a generic mesoscopic circuit. An example of expression for $\check{G}$ will be given in section IV for a non-interacting double dot.

The light matter coupling occurs in Eq.(22) through the term

$$\check{v}(\bar{\varphi},\varphi,t) = \check{g}\frac{\bar{\varphi}_{cl}(t)+\varphi_{cl}(t))\check{\sigma}_0 + (\bar{\varphi}_q(t)+\varphi_q(t))\check{\sigma}_1}{\sqrt{2}} \tag{27}$$

Above, we use matrices $\check{\sigma}_{0[1]} = \mathring{\sigma}_{0[1]}\otimes\widetilde{1}$, where $\mathring{\sigma}_0$ and $\mathring{\sigma}_1$ correspond to the identity and the first Pauli matrix in the Keldysh subspace of the mesoscopic circuit (index 0/1) and $\widetilde{1}$ is the identity in the mesoscopic orbitals subspace. We also note $\check{g} = \mathring{\sigma}_0\otimes\tilde{g}$ with $\tilde{g} = diag[g_1,...,g_N]$ a diagonal matrix in the mesoscopic orbitals subspace. More generally, the superscripts $\circ$ and $\sim$ decorate a matrix in the 2×2 mesoscopic Keldysh subspace and the $N\times N$ mesoscopic orbital subspace, respectively. The superscript $\vee$ decorates a matrix in the tensor product of these two spaces. The notation g used previously corresponds to $g = \max_d[g_d]$.

B. Effective cavity action to fourth order in $\check{g}/\omega_0$

In order to obtain an effective description of the cavity dynamics solely, one must integrate out the electronic degrees of freedom in Eq.(17). For simplicity, we will disregard Coulomb interactions in the mesoscopic circuit. In this case, the mesoscopic QED action is quadratic with respect the electronic fields ψ and $\bar{\psi}$, and one can thus perform a straightforward Gaussian integration of Eq.(17) on these fields (in the interacting case, it is possible to use more elaborate integration procedures[39]). The resulting effective cavity action $S_{cav}^{eff}(\bar{\varphi},\varphi)$ can be simplified after a systematic expansion with respect to the light/matter coupling matrix $\check{g}$ (see Appendix A for details). We work to fourth order in $\check{g}/\omega_0$ in order to capture essential non-linear electron/photon interaction effects. In order to simplify the final expression of S_{cav}^{eff}, we assume that the dressed cavity linewidth is much smaller than ω_0 and the width of the mesoscopic resonances linewidth. This criterion is largely satisfied in experiments as well as for the parameters used in this manuscript. We finally obtain the expression

$$S_{cav}^{eff}(\bar{\varphi},\varphi) = S_{cav}^{0}(\bar{\varphi},\varphi) + \sum_{i\in\{2,3,4\}} \Delta S_g^{(i)}(\bar{\varphi},\varphi) + o(\check{g}^4) \tag{28}$$

Above, $\Delta S_g^{(i)}$ is the mesoscopic circuit contribution to S_{cav}^{eff} to i^{th} order in $\check{g}/\omega_0$. The first order contribution in $\check{g}/\omega_0$ can be disregarded because it is not resonant with the cavity.

The second order contribution

$$\Delta S_g^{(2)}(\bar{\varphi},\varphi) = -\int_t \begin{bmatrix}\bar{\varphi}_{cl} & \bar{\varphi}_q\end{bmatrix}\cdot\begin{bmatrix}0 & \chi_2^* \\ \chi_2 & \lambda_2\end{bmatrix}\cdot\begin{bmatrix}\varphi_{cl}\\ \varphi_q\end{bmatrix} \tag{29}$$

involves the semiclassical charge susceptibility

$$\chi_2 = -\frac{i}{2}\int\limits_{\omega} \underset{d}{\mathrm{Tr}}\left[\tilde{G}_K(\omega)\tilde{g}\left(\tilde{G}_a(\omega-\omega_0)+\tilde{G}_r(\omega+\omega_0)\right)\tilde{g}\right] \tag{30}$$

of the mesoscopic circuit at frequency ω_0 and the correlation function

$$\begin{aligned}\lambda_2 = -\frac{i}{2}\int\limits_{\omega} \underset{d}{\mathrm{Tr}}[&\tilde{G}_K(\omega)\tilde{g}\tilde{G}_K(\omega+\omega_0)\tilde{g} \\ &+ \tilde{G}_a(\omega)\tilde{g}\tilde{G}_r(\omega+\omega_0)\tilde{g} + \tilde{G}_r(\omega)\tilde{g}\tilde{G}_a(\omega+\omega_0)\tilde{g}]\end{aligned} \tag{31}$$

We note $\int\limits_{\omega} = \int\limits_{-\infty}^{+\infty}\frac{d\omega}{2\pi}$, and $\underset{d}{\mathrm{Tr}}$ the trace operator on the mesoscopic orbital index d. Note that χ_2 has already been introduced in other works[22,29–32,38,50], essentially for studying the semiclassical behavior of a Mesoscopic QED device to second order in $\check{g}/\omega_0$. A cavity frequency shift is caused by $\mathrm{Re}[\chi_2]$ whereas $\mathrm{Im}[\chi_2]$ renormalizes the bare cavity linewidth Λ_0 of Eq.(19). The parameter λ_2 is necessary to describe the quantum regime of Mesoscopic QED, but it has been disregarded so far. From Eq.(31)

with $\tilde{G}_K(\omega) = -\tilde{G}_K(\omega)^\dagger$ and $\tilde{G}_a(\omega) = \tilde{G}_r(\omega)^\dagger$, one can check that λ_2 is purely imaginary.

For $\varepsilon_p \neq 0$, we obtain a third order term $S_g^{(3)}(t)$ in $\check{g}/\omega_0$ which can be expressed as

$$\Delta S_g^{(3)}(\bar{\varphi},\varphi) = -i\int_t e^{-2i\omega_0 t}\begin{bmatrix}\bar{\varphi}_{cl} & \bar{\varphi}_q\end{bmatrix}\cdot\begin{bmatrix}0 & U_{cl}/2\\ U_{cl}/2 & U_q\end{bmatrix}\cdot\begin{bmatrix}\bar{\varphi}_{cl}\\ \bar{\varphi}_q\end{bmatrix} - i\int_t e^{2i\omega_0 t}\begin{bmatrix}\varphi_{cl} & \varphi_q\end{bmatrix}\cdot\begin{bmatrix}0 & -U_{cl}^*/2\\ -U_{cl}^*/2 & U_q^*\end{bmatrix}\cdot\begin{bmatrix}\varphi_{cl}\\ \varphi_q\end{bmatrix} \tag{32}$$

with

$$U_{cl} = -\frac{\beta_p}{2}\int_\omega \underset{k,d}{\mathrm{Tr}}[\check{\sigma}_1\check{g}\check{G}(\omega)\check{g}\check{G}(\omega+\omega_0)\check{g}\check{G}(\omega-\omega_0)] + \underset{k,d}{\mathrm{Tr}}[\check{G}(\omega)\check{\sigma}_1\check{g}\check{G}(\omega+\omega_0)\check{g}\check{G}(\omega-\omega_0)\check{g}]) \tag{33}$$

$$U_q = -\frac{\beta_p}{2}\int_\omega \underset{k,d}{\mathrm{Tr}}[\check{\sigma}_1\check{g}\check{G}(\omega)\check{\sigma}_1\check{g}\check{G}(\omega+\omega_0)\check{g}\check{G}(\omega-\omega_0)] \tag{34}$$

and

$$\beta_p = \varepsilon_p t_0/2 \tag{35}$$

Above, we note $\underset{k,d}{\mathrm{Tr}}$ the trace operator on both the mesoscopic orbital index d and the Keldysh index k. The prefactor

$$t_0 = \mathcal{G}_0^r(2\omega_0) + \mathcal{G}_0^a(-2\omega_0) \tag{36}$$

takes into account how the mesoscopic circuit feels the ac drive through the cavity, with

$$\mathcal{G}_0^{r/a}(\omega) = (\omega - \omega_0 \pm i\frac{\Lambda_0}{2})^{-1} \tag{37}$$

the bare cavity retarded/advanced Green's function [see Eq.(110) for a semiclassical picture of this effect]. Subsequently, the reaction of the mesoscopic circuit to the ac drive affects the cavity effective behavior, as described by the terms in U_q and U_{cl}. Importantly, these terms can be significant because the smallness of t_0 can be compensated by the use of a large enough drive amplitude β_p. Interestingly, the coefficient U_{cl} corresponds to the semiclassical joint response of the mesoscopic charge to the cavity field in $\hat{a}$ and to the drive in β_p (see Appendix B1, Eq.(114)).

Finally, we find a fourth order contribution in $\check{g}/\omega_0$, which occurs even for $\beta_p = 0$, i.e.

$$\Delta S_g^{(4)}(\bar{\varphi},\varphi) = -\int_t \begin{bmatrix}\bar{\varphi}_{cl}\bar{\varphi}_{cl} & \bar{\varphi}_{cl}\bar{\varphi}_q & \bar{\varphi}_q\bar{\varphi}_q\end{bmatrix}.\mathcal{A}.\begin{bmatrix}\varphi_{cl}\varphi_{cl}\\ \varphi_{cl}\varphi_q\\ \varphi_q\varphi_q\end{bmatrix} \tag{38}$$

with

$$\mathcal{A} = \begin{bmatrix}0 & \chi_4^* & -U_4^*\\ \chi_4 & \lambda_4 & V_4^*\\ U_4 & V_4 & W_4\end{bmatrix} \tag{39}$$

$$\chi_4 = i(\mathcal{N}_{q,cl,cl,cl} + \mathcal{N}_{cl,q,cl,cl}) \tag{40}$$

$$\lambda_4 = i(\mathcal{N}_{cl,q,cl,q} + \mathcal{N}_{cl,q,q,cl} + \mathcal{N}_{q,cl,cl,q} + \mathcal{N}_{q,cl,q,cl}) \tag{41}$$

$$V_4 = i(\mathcal{N}_{q,q,cl,q} + \mathcal{N}_{q,q,q,cl}) \tag{42}$$

$$U_4(\omega_0) = i\mathcal{N}_{q,q,cl,cl} \tag{43}$$

$$W_4(\omega_0) = i\mathcal{N}_{q,q,q,q} \tag{44}$$

$$\mathcal{N}_{f,f',l,l'} = -\int_\omega \underset{k,d}{\mathrm{Tr}}\left[\frac{1}{8}\check{G}(\omega)\hat{\sigma}_f\check{g}\check{G}_+\hat{\sigma}_l\check{g}\check{G}(\omega)\hat{\sigma}_{f'}\check{g}\check{G}_+\hat{\sigma}_{l'}\check{g} + \frac{1}{4}\check{G}(\omega)\hat{\sigma}_f\check{g}\check{G}_+\hat{\sigma}_{f'}\check{g}\check{G}(\omega+2\omega_0)\hat{\sigma}_l\check{g}\check{G}_+\hat{\sigma}_{l'}\check{g}\right] \tag{45}$$

and $\check{G}_+ = \check{G}(\omega+\omega_0)$. Note that λ_4 and W_4 are purely imaginary due to $\tilde{G}_K(\omega) = -\tilde{G}_K(\omega)^\dagger$ and $\tilde{G}_a(\omega) = \tilde{G}_r(\omega)^\dagger$. The coefficient χ_4 corresponds to the second order semiclassical response function of the quantum dot to the cavity electric field (see Appendix B1, Eq.(114)). The other coefficients λ_4, U_4, V_4 and W_4 are necessary to describe quantum fluctuations of the cavity field. In summary, Eqs. (28) - (45) describe the effective action of a microwave cavity in a generic Mesoscopic QED device to fourth order in the light/matter coupling. This requires to introduce new types of quantum dot correlators than the known χ_2. We will discuss the physical effect of the new correlators λ_2, U_{cl}, U_q, χ_4, λ_4, U_4, V_4 and W_4 in the next sections. Importantly, one has to choose an appropriate technique to obtain an explicit description of the cavity dynamics out of the cavity effective action. In the following we will consider Markovian situations such that an effective Lindblad equation on the cavity density matrix can be used.

C. Correspondence between the cavity effective action and a photonic Lindblad equation

The most popular description of Circuit QED is the Lindblad equation which describes the evolution of the cavity density matrix. Below, we come back to this description to clarify the physical meaning of the different terms in the cavity action.

1. *Cavity effective Lindblad equation up to third order in $\check{g}/\omega_0$*

In the limit of low couplings g_d and limited cavity drive β_p, the cavity field remains small so that one can truncate the cavity effective action to third order in $\check{g}/\omega_0$. In this

case, we show below that it is always possible to establish a Markovian Lindblad equation on the cavity density matrix. Thereby, we clarify the physical meaning of the terms in U_{cl} and U_q.

When a cavity follows a Markovian evolution, the time derivative of its density matrix $\rho_{cav}(t)$ only depends on the value of ρ_{cav} at time t. More precisely, one can use a Lindblad equation[15]:

$$\frac{\partial \rho_{cav}(t)}{\partial t} = -i[H_{cav}^{eff}, \rho_{cav}(t)] + \gamma_j \mathcal{L}_{\hat{L}_j}(\rho_{cav}(t)) \quad (46)$$

with H_{cav}^{eff} the effective cavity Hamiltonian, γ_j the rate of a dissipative process corresponding to the jump operator $\hat{L}_j$ and $\mathcal{L}_{\hat{L}_j}(\rho_{cav})$ defined in Eq.(13). Let us assume that the effective Hamiltonian has the generic form

$$H_{cav}^{eff} = (\omega_0 + \Delta\omega_0)\hat{a}^\dagger \hat{a} + i\rho_p e^{-i2\omega_0 t}\hat{a}^{\dagger 2} - i\rho_p^* e^{i2\omega_0 t}\hat{a}^2 \quad (47)$$

and the dissipative processes are characterized by $(\gamma_j, \hat{L}_j) \in \mathcal{P}$ with

$$\mathcal{P} = \{(\gamma_{loss}, \hat{a}), (\gamma_{gain}, \hat{a}^\dagger), (\gamma_p, \hat{a} + e^{i\varphi_p} e^{-i2\omega_0 t}\hat{a}^\dagger)\} \quad (48)$$

The above parameters $\Delta\omega_0$, ρ_p, γ_{loss}, γ_{gain} and γ_p are unspecified for the moment. The action corresponding to the master equation (46) can be expressed as (see details in Appendix C)

$$\begin{aligned} S_{Mark}(t) = &\int_t \begin{bmatrix} \bar{\varphi}_{cl} & \bar{\varphi}_q \end{bmatrix} \cdot \begin{bmatrix} 0 & F_t - i\frac{\gamma_-}{2} \\ F_t + i\frac{\gamma_-}{2} & i\gamma_+ \end{bmatrix} \cdot \begin{bmatrix} \varphi_{cl} \\ \varphi_q \end{bmatrix} \\ &+ \int_t e^{-i2\omega_0 t} \begin{bmatrix} \bar{\varphi}_{cl} & \bar{\varphi}_q \end{bmatrix} \cdot \begin{bmatrix} 0 & -i\rho_p \\ -i\rho_p & i\gamma_p e^{i\varphi_p} \end{bmatrix} \cdot \begin{bmatrix} \bar{\varphi}_{cl} \\ \bar{\varphi}_q \end{bmatrix} \\ &+ \int_t e^{i2\omega_0 t} \begin{bmatrix} \varphi_{cl} & \varphi_q \end{bmatrix} \cdot \begin{bmatrix} 0 & i\rho_p^* \\ i\rho_p^* & i\gamma_p e^{-i\varphi_p} \end{bmatrix} \cdot \begin{bmatrix} \varphi_{cl} \\ \varphi_q \end{bmatrix} \end{aligned} \quad (49)$$

with

$$\gamma_- = \gamma_{loss} - \gamma_{gain} \quad (50)$$

$$\gamma_+ = \gamma_{loss} + \gamma_{gain} + 2\gamma_p \quad (51)$$

and $F_t = i\partial t - \omega_0 - \Delta\omega_0$. It is possible to perform an exact identification between the actions of Eqs.(49) and (28) to third order in $\check{g}/\omega_0$ by using

$$\Delta\omega_0 = \mathrm{Re}[\chi_2] \quad (52)$$

$$\rho_p = U_{cl}/2 \quad (53)$$

$$\gamma_p e^{i\varphi_p} = -U_q \quad (54)$$

$$\gamma_{loss} = \gamma_{loss}^0 - \gamma_p \quad (55)$$

$$\gamma_{gain} = \gamma_{gain}^0 - \gamma_p \quad (56)$$

with

$$\gamma_{loss}^0 = \Lambda_0(1 + n_B) - \mathrm{Im}[\chi_2 + \frac{\lambda_2}{2}] \quad (57)$$

$$\gamma_{gain}^0 = \Lambda_0 n_B + \mathrm{Im}[\chi_2 - \frac{\lambda_2}{2}] \quad (58)$$

and $\gamma_p > 0$ by definition.

We now comment on the physical effect of the components (52)-(58). As found previously[22,29–32,38,50], the cavity frequency shift $\Delta\omega_0$ is directly set by the real part of χ_2. A comparison between Eqs.(19) and (49) indicates that the cavity intrinsic linewidth Λ_0 is also shifted by $\Delta\Lambda_0 = -2\,\mathrm{Im}[\chi_2]$. The dissipative processes with rates γ_{loss} and γ_{gain} correspond to standard single photon emission and absorption which are widely considered in circuit QED. One can see from Eqs.(55)-(58) that $Im[\chi_2]$ contributes to the asymmetry between the photon loss and gain rates γ_{loss} and γ_{gain} whereas $Im[\lambda_2]$ contributes equally to γ_{loss} and γ_{gain}. The coefficients ρ_p and γ_p account for the effect of the ac drive since they are nonzero only for $\beta_p \neq 0$. From Eq.(53), U_{cl} generates the two-photon coherent drive in ρ_p of Eq.(47). In Circuit QED, a similar drive has been recently obtained by using a complex configuration with two microwave cavities coupled nonlinearly and subject to two off resonant drives[6]. Finally, the process with a rate γ_p generated by U_q has not been considered so far and seems more specific to strongly dissipative structures. Its jump operator $L_p = \hat{a} + e^{i\varphi_p} e^{-i2\omega_0 t}\hat{a}^\dagger$ corresponds to an unusual time-dependent coherent superposition of photon absorption and emission operators. From Eqs. (55) and (56), one could believe that γ_p decreases the single photon loss and gain rates, but this is not effective because the rates γ_+ and γ_- through which γ_{loss} and γ_{gain} occur in the cavity action do not depend on γ_p. Indeed, from Eqs.(50), (51), (55) and (56), one has $\gamma_- = \gamma_{loss}^0 - \gamma_{gain}^0$ and $\gamma_+ = \gamma_{loss}^0 + \gamma_{gain}^0$. There remains a term in γ_p which occurs through the second and third lines of Eq.(49) on the same footing as ρ_p. We will study the effect of this peculiar term in section IV D 2 for the case of a double quantum dot and show that it corresponds to a "squeezing dissipation". Importantly, in this work, we have used a range of γ_p such that one has $\gamma_{loss} > 0$ and $\gamma_{gain} > 0$, as required by the definition of the Markovian Lindblad equation (46). When the drive amplitude β_p becomes so large that $\gamma_{loss} < 0$ and/or $\gamma_{gain} < 0$, we expect that higher order terms in β_p become relevant, which introduces new terms in the cavity action which are not necessarily Markovian. In this case, the Lindblad Eq.(46) is not relevant anymore. This limit is beyond the scope of this article.

2. Cavity effective Lindblad equation to fourth order in $\check{g}/\omega_0$

We now investigate the possibility to identify the path integral approach of section III with a Lindblad description up to fourth order in $\check{g}/\omega_0$. We expect an extra contribution

$$H_{cav}^{eff,4} = K\hat{a}^{\dagger 2}\hat{a}^2 \tag{59}$$

to the effective Hamiltonian (47), which corresponds to a Kerr photonic interaction. We also expect dissipative processes with rates and jump operators $(\gamma_j, \hat{L}_j) \in \mathcal{P}_4$ with

$$\mathcal{P}_4 = \{(K_{loss}, \hat{a}^2), (K_{gain}, \hat{a}^{\dagger 2}), (D, \hat{a}^\dagger \hat{a})\} \tag{60}$$

The three processes in the above ensemble correspond respectively to two photon loss, two photon gain and pure dephasing. This leads to an action contribution (see Appendix A)

$$S_{Mark}^{(4)} = -\int_t \left[\bar{\varphi}_{cl}\bar{\varphi}_{cl} \;\; \bar{\varphi}_{cl}\bar{\varphi}_q \;\; \bar{\varphi}_q\bar{\varphi}_q\right] . \mathcal{A}_M . \begin{bmatrix} \varphi_{cl}\varphi_{cl} \\ \varphi_{cl}\varphi_q \\ \varphi_q\varphi_q \end{bmatrix} \tag{61}$$

with

$$\mathcal{A}_M = \begin{bmatrix} 0 & i\frac{K_-}{2} + K & -\frac{iD}{2} \\ -i\frac{K_-}{2} + K & -i\,(D + 2K_+) & -i\frac{K_-}{2} + K \\ -\frac{iD}{2} & i\frac{K_-}{2} + K & 0 \end{bmatrix} \tag{62}$$

and $K_- = K_{loss} - K_{gain}$, $K_+ = K_{loss} + K_{gain}$. To establish a mapping with the path integral description, we now have to compare the above matrix $\mathcal{A}_M$ with the matrix $\mathcal{A}$ of Eq. (39) which occurs in the effective action of the Mesoscopic QED device to fourth order in $\check{g}/\omega_0$. Strikingly, $\mathcal{A}_M$ and $\mathcal{A}$ cannot be mapped in all situations. This is rigorously possible when the condition

$$\mathcal{C}_{Mark} = (W_4 = 0)\&(\mathrm{Re}[U_4] = 0)\&(V_4 = \chi_4^*) \tag{63}$$

is fulfilled. Equation (63) represents a sufficient condition to have a Markovian cavity dynamics to fourth order in $\check{g}/\omega_0$. For a given mesoscopic circuit, one must test this condition by evaluating numerically the different fourth order mesoscopic correlators. When condition (63) is valid, one has

$$K = \mathrm{Re}[\chi_4] \tag{64}$$

$$K_{loss/gain} = \mp\,\mathrm{Im}[\chi_4] + \frac{\mathrm{Im}[U_4]}{2} - \frac{\mathrm{Im}[\lambda_4]}{4} \tag{65}$$

and

$$D = -2\,\mathrm{Im}[U_4] \tag{66}$$

Hence, $\mathrm{Re}[\chi_4]$ generates the effective Kerr interaction (59). Remarkably, there exists an analogy between the expressions of the rates for the single and two photon stochastic processes, Eqs. (65) and Eqs. (57)-(58). Indeed, $\mathrm{Im}[\chi_4]$ provides an opposite contribution to two-photon loss and gain, like $\mathrm{Im}[\chi_2]$ does for single photon processes. In contrast, $\mathrm{Im}[\lambda_4] - 2\,\mathrm{Im}[U_4]$ provides the same contribution to two-photon loss and gain, like $\mathrm{Im}[\lambda_2]$ does for single photon processes. The term in $\mathrm{Im}[U_4]$ also contributes to photonic dephasing (term in D). This last effect does not have any analogue to second order in $\check{g}/\omega_0$.

We could not find other contributions to the jump operator ensemble $\mathcal{P}_4$ of Eq. (60) to extend the mapping between the path integral approach and the Lindblad description beyond the regime of validity of Eq.(63). Anyhow, to fourth order in $\check{g}/\omega_0$, a full mapping cannot be expected since the dynamics of the cavity is not necessarily Markovian. For instance, there can be "memory" effects due to a coherent exchange of energy between the cavity and the mesoscopic circuit. This will be illustrated in the case of a non-interacting double quantum dot in section IV E.

3. Summary: total photonic Lindblad equation up to fourth order in $\check{g}/\omega_0$ in the interaction picture

In practice, it is convenient to study the cavity dynamics in an interaction picture by considering the time evolution of the cavity density operator $\rho_{cav}^I(t) = e^{i\omega_0\hat{a}^\dagger\hat{a}t}\rho_{cav}(t)e^{-i\omega_0\hat{a}^\dagger\hat{a}t}$. In this picture, Eqs. (46), (47), (48), (59) and (60) lead to

$$\frac{\partial\rho_{cav}^I(t)}{\partial t} = -i[H_{cav}^{eff,I}, \rho_{cav}^I] + \gamma_j\mathcal{L}_{\hat{L}_j}(\rho_{cav}^I) \tag{67}$$

with

$$H_{cav}^{eff,I} = \Delta\omega_0\hat{a}_I^\dagger\hat{a}_I + i\rho_p\hat{a}_I^{\dagger 2} - i\rho_p^*\hat{a}_I^2 + K\hat{a}_I^{\dagger 2}\hat{a}_I^2 \tag{68}$$

and dissipative processes $(\gamma_j, \hat{L}_j) \in \mathcal{P}_I$ with

$$\begin{aligned}\mathcal{P}_I = \{&(\gamma_{loss}, \hat{a}_I), (\gamma_{gain}, \hat{a}_I^\dagger), (\gamma_p, \hat{a}_I + e^{i\varphi_p}\hat{a}_I^\dagger), \\ &(K_{loss}, \hat{a}_I^2), (K_{gain}, \hat{a}_I^{\dagger 2}), (D, \hat{a}_I^\dagger\hat{a}_I)\}\end{aligned} \tag{69}$$

with $\hat{a}_I = e^{-i\omega_0 t}\hat{a}$.

Interestingly, Eq.(67) appears as a generalization to fourth order in $\check{g}/\omega_0$ of Eq.(12) obtained with the direct density matrix approach. Indeed, one can check that these two Eqs. agree to second order in $\check{g}/\omega_0$, provided the assumption $\Lambda_0 = 0$ of section II B is used. For this purpose, one must use the equalities

$$\chi_2 = \chi_B(\omega_0) - \chi_A(\omega_0) \tag{70}$$

and

$$\lambda_2|_{\omega_0\neq 0} = 2i\,\mathrm{Im}\left[\chi_A(\omega_0) + \chi_B(\omega_0)\right] \tag{71}$$

which are derived in Appendix D.

IV. THE CASE OF A DOUBLE QUANTUM DOT IN A CAVITY

A. Circuit description

We now apply the results of section III to the case of a spin-degenerate double quantum dot coupled to a microwave cavity, represented schematically in Fig.I, panels (a) and (b). This circuit encloses two quantum dots L and R with a tunnel coupling t_{LR} such that $\hat{H}_{meso}$ includes a term $t_{LR}\hat{c}_L^\dagger\hat{c}_R + t_{LR}^*\hat{c}_R^\dagger\hat{c}_L$. The dot $L(R)$ is contacted to a normal metal reservoir with a tunnel rate $\Gamma_{L(R)}$. Equation (1) gives $\Gamma_d = 2\pi\Sigma_{k\in C}\left|t_{k,d}\right|^2$ for $d \in L(R)$. The rate Γ_d can be considered as energy-independent in the framework of a wide band approximation for the reservoirs with $\left|t_{k,d}\right|^2$ independent of k. In the following we consider the case $\Gamma_L = \Gamma_R = \Gamma$. A bias voltage V is applied between the two normal metal contacts. The orbital energy $\omega_{L(R)}$ of dot $L(R)$ can be finely tuned with an electrostatic gate. In principle, $\omega_{L(R)}$ can also be shifted by a fraction of eV which depends on the ratio of the junctions capacitances. Here we will assume that this shift is negligible[51]. We will also disregard Coulomb interactions in the double dot. This basic case presents essential ingredients of mesoscopic QED: the cavity electric field can couple to both the internal transition between the L and R orbitals of the double dot, and to transitions between the dots and the continuum of states of the normal metal reservoirs.

B. Unperturbed mesoscopic Green's function of the double dot

The unperturbed mesoscopic circuit Green's function $\check{G}$ of the double dot, whose inverse appears in Eq. (21), must be calculated in the absence of light/matter coupling (i.e. $g_L = 0$ and $g_R = 0$). It can be obtained by performing the inversion

$$\check{G}(\omega) = \begin{bmatrix} \tilde{G}_r^{-1}(\omega) & \tilde{M}_K \\ \tilde{0} & \tilde{G}_a^{-1}(\omega) \end{bmatrix}^{-1} \tag{72}$$

with[52,53]

$$\tilde{G}_{r(a)}^{-1}(\omega) = \begin{bmatrix} \omega - \omega_L \pm i\frac{\Gamma}{2} & -t_{LR} \\ -t_{LR}^* & \omega - \omega_R \pm i\frac{\Gamma}{2} \end{bmatrix} \tag{73}$$

and

$$\tilde{M}_K = \begin{bmatrix} i\Gamma(1-2n_{F,L}(\omega)) & 0 \\ 0 & i\Gamma(1-2n_{F,R}(\omega)) \end{bmatrix} \tag{74}$$

Equations (73) and (74) stem from the explicit definitions (24)-(26) of the Green's functions $\tilde{G}_{r/a/K}(\omega)$ in terms of fermionic operators and the expression of the double dot circuit Hamiltonian (see Eq. (2) with $g_{L(R)} = 0$). Since we consider a spin degenerate situation with non-interacting quantum dots, the spin degree of freedom is omitted in the above orbital subspace structure. We will restore it later in numerical evaluations by taking into account an implicit multiplication by a factor 2 in the traces operator over the orbital index d. The Fermi occupation function $n_{F,L(R)}(\omega) = (1 + \exp[(\omega \mp (eV_b/2))/k_BT])^{-1}$ of the $L(R)$ contact is affected by the bias voltage V_b. For later use, we also define the lesser self energy of the double dot[52]

$$\tilde{\Sigma}^<(\omega) = \begin{bmatrix} i\Gamma n_{F,L}(\omega) & 0 \\ 0 & i\Gamma n_{F,R}(\omega) \end{bmatrix} \tag{75}$$

and the light/matter coupling matrix

$$\check{g} = diag[g_L, g_R, g_L, g_R] \tag{76}$$

C. Choice of parameters

For simplicity, we will use a nonzero g_L and $g_R = 0$, which corresponds to DQD experiments realized so far, where a very asymmetric microwave coupling to the two dots is engineered. In experiments realized with standard coplanar microwave resonators, the light matter coupling is typically $g_L \sim 0.001\omega_0$[17]. In a more recent design based on high kinetic inductance superconducting nanowire resonators, $g_L \sim 0.03\omega_0$ was reached[54]. However, since the rms voltage of these resonators is[55] $V_{rms} = 20\ \mu V \simeq 4.9$ GHz for $\omega_0 \sim 4$ GHz, one can reach $g_L \sim \omega_0$, in principle, by using a galvanic coupling between one of the dots and the cavity.

Since we develop the cavity action with respect to g_L and β_p, the amplitude of these parameters must not be too large. First, in the absence of ac drive, the cavity effective action has contributions in g_L^{2n} only, with $n \in \mathbb{N}$. One must use $g_L/\omega_0 \leqslant 0.5$ so that contributions with $n > 4$ remain negligible. Second, when the ac drive is switched on ($\beta_p \neq 0$), action contributions in g_L^{2n+1} appear. We will only take into account the lowest order contribution, corresponding to Eq.(32), which is in $\beta_p g_L^3$. We will use $\beta_p g_L^3/\omega_0^3 \ll 1$ so that higher order contributions in β_p are expected to be negligible.

D. The low coupling limit: squeezed photonic vacuum induced by a double quantum dot

1. *Evaluation of the Lindblad equation coefficients to third order in g_L/ω_0*

We have seen above that U_{cl} corresponds to a coherent two photon drive whereas U_q corresponds to an unusual form of dissipation. In this section, we evaluate these coefficients in the double dot case. Figure 3 shows $|U_{cl}|$ and $|U_q|$ versus the dot orbital energies ω_L and ω_R, for moderate tunnel rates $\Gamma = 0.1\omega_0$ and a moderate interdot hopping $t_{LR} = 0.1\omega_0$. We use a zero bias voltage in panels (a) and (b) and a nonzero bias voltage $V_b = 1.5\omega_0$ in panels (c) and (d). Both U_{cl}

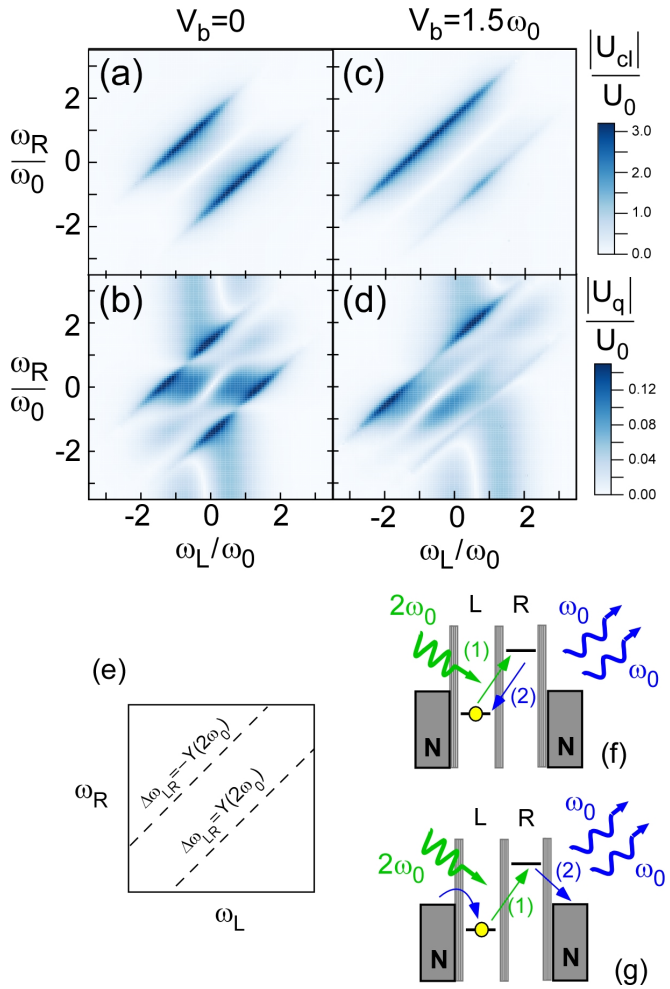

FIG. 3: Panels (a), (b), (c) and (d): Absolute values of the coefficients U_{cl} and U_q which account for the effect of the $2\omega_0$ drive of the cavity at order 3 in the photon/dot coupling g, versus the dot orbital energies ω_L and ω_R. Panels (a) and (b) correspond to a bias voltage $V_b = 0$ and panels (c) and (d) to $eV_b = 1.5\omega_0$. The other parameters are $\Gamma = 0.1\omega_0$, $t_{LR} = 0.7\omega_0$, $k_BT = 0.275\omega_0$, $g_R = 0$, and $\Lambda_0 = 5.10^{-5}\omega_0$. We use a normalization factor $U_0 = g_L^3\beta_p/\omega_0^2$. Panel (e) indicates the positions of resonances between the dot internal degree of freedom and the cavity for $\Delta\omega_{LR} \simeq \pm R(2\omega_0)$. Panels (f) and (g): examples of coherent and dissipative processes in g_L^3 involving the $2\omega_0$ drive. When the internal transition of the double dot matches $2\omega_0$, it can absorb a $2\omega_0$ photon. This enables the emission of two ω_0 photons upon electronic transitions which are internal to the dot (panel (f)) or involve the normal metal contacts (panel (g)).

and U_q show strong resonances which appear as diagonal lines in Fig.3. These lines correspond to resonances of the cavity with the double dot internal degree of freedom (see panel (e)). More precisely, the bonding and antibonding states of the double dot, which result from the tunnel coupling between the left and right orbitals, have energies $\omega_\mp = (\omega_L + \omega_R \mp \sqrt{\Delta\omega_{LR}^2 + 4t_{LR}^2})/2$ with $\Delta\omega_{LR} = \omega_L - \omega_R$ the dots orbital detuning. In principle, single photon resonances $\omega_+ - \omega_- = \omega_0$ are expected for $\Delta\omega_{LR} = \pm Y(\omega_0)$ with $Y(\omega_0) = \sqrt{\omega_0^2 - 4t_{LR}^2}$, and two-photon resonances are expected for $\Delta\omega_{LR} = \pm Y(2\omega_0)$. In Fig.3, only the two-photon resonances are visible because we use $2t_{LR} > \omega_0$ and therefore the condition $\Delta\omega_{LR} = \pm Y(\omega_0)$ can never be satisfied. Panels (f) and (g) show some examples of two-photon processes which are expected to contribute to the resonances at $\Delta\omega_{LR} = \pm Y(2\omega_0)$. A photon with frequency $2\omega_0$ can be converted into two photons with frequency ω_0, in tunneling sequences which can be either purely coherent (panel (f)) or dissipative (panel (g)). Interestingly, the gate voltage area where the two-photon resonances appear is modified when a nonzero bias voltage is used (panels (c) and (d)). This is because the third order processes such as the one of panels (f) and (g) require that the double dot bonding and antibonding states are occupied and empty respectively, and the transport processes induced by a nonzero V_b modify the occupation of these states. Therefore using a nonzero bias voltage can be useful to trigger two-photon processes, especially in case of weak tunability of $\omega_{L(R)}$, which can happen for some types of quantum dots. Interestingly, $|U_q|$ also shows broad vertical resonances (for ω_L constant) outside of the gap between the $\Delta\omega_{LR} = Y(2\omega_0)$ and $\Delta\omega_{LR} = -Y(2\omega_0)$ resonances (see panels (b) and (d)). These resonances are due to tunneling between the left dot and the left reservoir, due to the conditions $g_L \neq 0$ and $\Gamma \neq 0$. As expected, these resonances shift with V_b (compare panels (b) and (d)) and get thinner when Γ decreases (not shown). The transition between the right reservoir and the right dot is not directly coupled to the cavity since $g_R = 0$, but a broad horizontal resonance also appears in Fig.3b between the lines $\Delta\omega_{LR} = Y(2\omega_0)$ and $\Delta\omega_{LR} = -Y(2\omega_0)$ because the hybridization between the left and right orbitals enables tunneling to the right reservoir. Note that the horizontal and vertical resonances induced by the presence of the normal metal reservoirs are visible in $|U_q|$ but not in $|U_{cl}|$. This can be explained by the fact that tunneling to the normal metal reservoirs is a stochastic effect which impacts more directly the dissipative processes in γ_p (or U_q) than the coherent drive in ρ_p generated by U_{cl}.

2. *Stationary Wigner function of the cavity to third order in g_L/ω_0*

To characterize the effects of the terms in U_{cl} and U_q, we now calculate analytically the stationary cavity Wigner function which follows from Eq.(67) to third order in $\check{g}/\omega_0$, i.e. assuming that the terms in K, K_{loss}, K_{gain} and D are negligible. The cavity Wigner function can be defined quite generally as

$$W(\alpha,\alpha^*,t) = \frac{1}{\pi^2}\int d^2\beta e^{(\beta^*\alpha-\alpha^*\beta)}\left\langle e^{\beta\hat{a}_I^\dagger-\beta_I^*\hat{a}_I}\right\rangle_t \quad (77)$$

Following the method of Ref.[44], one can show that Eq. (67) leads to the evolution equation

$$\begin{aligned}\frac{\partial}{\partial t}W = &\left(-i\Delta\omega_0\left[\frac{\partial}{\partial\alpha^*}\alpha^* - \frac{\partial}{\partial\alpha}\alpha\right]\right)W \\ &+\left(\frac{\gamma_+}{2}\frac{\partial}{\partial\alpha}\frac{\partial}{\partial\alpha^*} + \frac{\gamma_-}{2}\left(\frac{\partial}{\partial\alpha}\alpha + \frac{\partial}{\partial\alpha^*}\alpha^*\right)\right)W \\ &-\left(2\rho_p\frac{\partial}{\partial\alpha}\alpha^* + 2\rho_p^*\frac{\partial}{\partial\alpha^*}\alpha\right)W \\ &-\gamma_p\left(\frac{e^{-i\varphi_p}}{2}\frac{\partial^2}{\partial\alpha^{*2}} + \frac{e^{i\varphi_p}}{2}\frac{\partial^2}{\partial\alpha^2}\right)W\end{aligned} \tag{78}$$

(see details in Appendix E). To our knowledge, the term in γ_p in Eq.(78) has not been considered before, in the context of Circuit or Cavity QED. In the stationary regime, the solution of this equation is:

$$W(\alpha,\alpha^*,t\to+\infty) = \frac{1}{\pi\sqrt{A^2-4\left|B\right|^2}}\exp\left(\frac{P}{A^2-4\left|B\right|^2}\right) \tag{79}$$

with

$$P = A\left|\alpha\right|^2 + B^*\alpha^2 + B\alpha^{*2} \tag{80}$$

and, to third order in $\check{g}/\omega_0$ and first order in ε_p,

$$A = -\gamma_+/2\gamma_- \tag{81}$$

and

$$B = \left(\rho_p\frac{\gamma_+}{\gamma_-} - \gamma_p\frac{e^{i\varphi_p}}{2}\right)/\left(\gamma_- + 2i\Delta\omega_0\right) \tag{82}$$

Equation (79) describes a squeezed cavity vacuum. The major axis of the squeezed Gaussian is tilted by an angle $\theta = \arg[B]/2$ from the Re$[\alpha]$ axis. The fields quadratures along the θ and $\theta+\pi/2$ angles have the variances $\Delta X_\pm = \sqrt{-(A/2)\pm|B|}$. Strinkingly, from Eq.(82), the coherent drive in ρ_p and the dissipation processes in γ_p can both contribute to cavity squeezing and interfere constructively or destructively depending on the value of the phase φ_p. Note that expression (79) is valid for any type of mesoscopic circuit as long as (67) can be treated to third order in $\check{g}/\omega_0$. In Appendix F, we study in more details the influence of the double dot parameters on the photonic squeezing.

E. Photonic Schrödinger cat states produced by a double quantum dot

Obtaining Schrödinger cat states is useful to study the quantum behavior of a device on a fundamental level as well as to develop quantum computers. To obtain such states with our device, we need to invoke the fourth order terms in g_L/ω_0 of Eqs. (59) or (60), which will generate multistability in the cavity behavior. For simplicity, we will perform the study of this situation in the particular case where the system dynamics remains Markovian. This limit presents the advantage of remaining formally simple while demonstrating interesting potentialities of Mesoscopic QED.

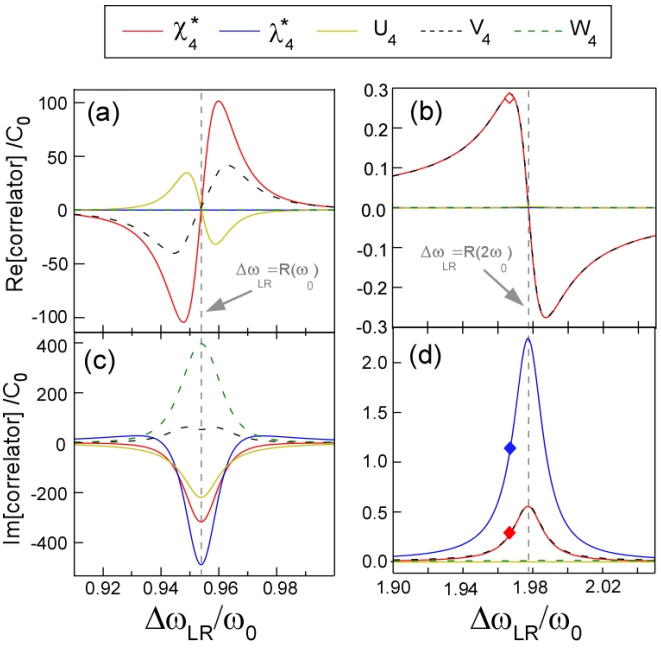

FIG. 4: Fourth order electronic correlation functions versus $\Delta\omega_{LR}$ calculated for $\omega_{av} = (\omega_L+\omega_R)/2 = 0.989\omega_0$, $\Gamma = 0.01\omega_0$, $t_{LR} = 0.15\omega_0$, $k_BT = 0.3\omega_0$, $eV_b = 0$, $g_R = 0$, $\beta_p = 0.35$, and $\Lambda_0 = 10^{-4}\omega_0$. Panels (a) and (b) show the real parts of the correlators and panels (c) and (d) the imaginary parts. The left panels show the area $\Delta\omega_{LR}\sim R(\omega_0)$ whereas the right panels show $\Delta\omega_{LR}\sim R(2\omega_0)$. All correlation functions are normalized by $C_0 = g_L^4/\omega_0^3$. The full and empty diamonds correspond to reference points for a comparison with Fig.5. The Markovian condition (63) is satisfied when the red full lines and black dashed lines coincide in the top and bottom panels ($\chi_4^* = V_4$), the green dashed line is close to 0 in both panels ($W_4 = 0$) and the yellow line is close to zero in the top panel (Re$[U_4] = 0$). This is true for panels (b) and (d).

1. *Double dot correlation functions to fourth order in g_L/ω_0*

In the double dot case, can the Markovian approximation hold to fourth order in g_L/ω_0, or equivalently, can the condition $\mathcal{C}_{Mark}$ of Eq.(63) be satisfied? To answer this question, we show in Fig.4 the dependence of the coefficients χ_4, λ_4, U_4, V_4 and W_4 on $\Delta\omega_{LR}$, for a zero bias voltage ($V_b = 0$) and low tunnel rates ($\Gamma = 0.01\omega_0$). Figures 4a and c show that $\mathcal{C}_{Mark}$ is not true when the double dot is resonant with the cavity ($\Delta\omega_{LR}\sim R(\omega_0)$). This is not surprising, because, in this case, real energy exchanges between the double dot and the cavity are possible, leading to vacuum Rabi oscillations in the case of

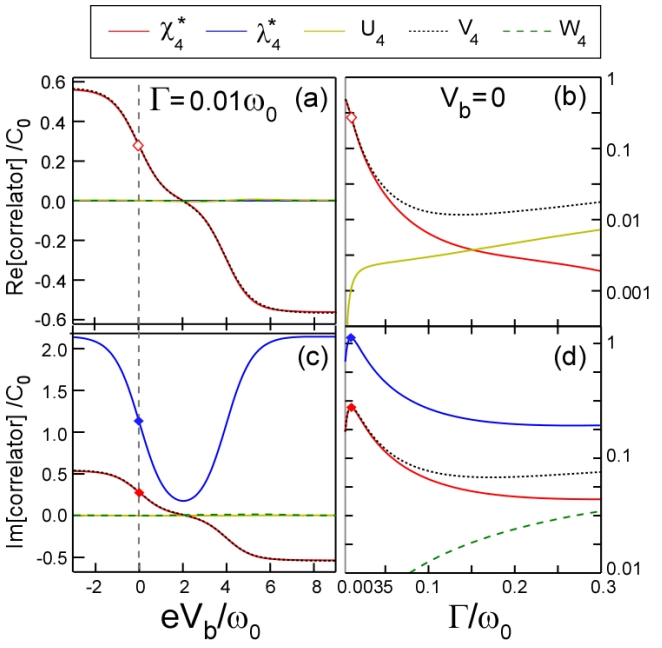

FIG. 5: Fourth order electronic correlation functions versus V_b for $\Gamma = 0.01\omega_0$ [panels (a) and (c)] and versus Γ for $V_b = 0$ [panels (b) and (d)]. We use $\omega_{av} = 0.989\omega_0$ and $\Delta\omega_{LR} = 1.967\omega_0$. The other parameters are the same as in Fig.4. The diamonds correspond to reference points identical to those of Fig.4.

low Γ and Λ_0. Hence, for the cavity, the mesoscopic circuit represents a "bath with memory", which is incompatible with an effective Markovian dynamics. Another interesting regime is $\Delta\omega_{LR} \sim \pm Y(2\omega_0)$, because the electronic correlation functions in g_L^4 present resonances in this area, as already seen for U_{cl} and U_q to third order in g_L/ω_0. The Markovian condition (63) is satisfied for $\Delta\omega_{LR} \sim \pm Y(2\omega_0)$, small values of Γ and t_{LR}, and $V_b = 0$ (Figs.4b and d) as well as a nonzero V_b (Figs.5a and 5c). One may attribute this result to the fact that, in this regime, there can only be virtual energy exchanges between the cavity and the double dot, which occur on a timescale which is very short in comparison with the typical timescale for the evolution of the cavity. The Markovian condition is not valid anymore for higher tunnel rates $\Gamma > 0.1\omega_0$ (see Figs.5b and 5d). Indeed, in this case the resonances at $\Delta\omega_{LR} \sim Y(\omega_0)$ and $\Delta\omega_{LR} \sim Y(2\omega_0)$ start overlapping and the distinction between real and virtual energy exchanges between the cavity and the double dot becomes less clear. The Markovian condition is not valid either for $\Delta\omega_{LR} \sim Y(2\omega_0)$ and t_{LR} large ($t_{LR} > 0.3\omega_0$) (not shown). This is why, in the rest of this section, we will focus on the Markovian dynamics of the cavity for $\Delta\omega_{LR} \sim Y(2\omega_0)$, $t_{LR} \lesssim 0.15\omega_0$ and $\Gamma \lesssim 0.1\omega_0$. Note that for $\Gamma \to 0$, the imaginary part of the correlators vanishes (see the very left of Fig.5d for the onset of this effect). Since we are interested in the effect of a genuinely dissipative mesoscopic circuit, we will only consider the case $\Gamma \geq 0.005\omega_0$ in the following. In particular, we will consider the working point $\Gamma \simeq 0.01\omega_0$ where $|\mathrm{Im}[\chi_4]|$ and $|\mathrm{Im}[\lambda_4]|$ have a local maximum (see very left of Fig.5d). Figure 6 represents some possible photonic processes at fourth order in g_L/ω_0 in this limit (see panels (a), (b_1), (b_2), (b_3) and (c)), for different configurations of dot orbital energies and bias voltage. It also shows K_{loss} and K_{gain} versus $\Delta\omega_{LR}$ and V_b for the parameters of Fig.4 and Fig.5 with $\Gamma = 0.01\omega_0$ and $\Delta\omega_{LR} = Y(2\omega_0)$. In these conditions, one can check that for $V_b = 0$, the two-photon stochastic dissipation rate K_{loss} is the dominant stochastic rate in Eq.(69), i.e. K_{gain}, D, γ_{loss} and γ_{gain} are much weaker. The rate K_{loss} corresponds to the type of processes represented in Fig.6, panels (b_1) and (b_2), where two photons can be absorbed simultaneously by the double dot circuit because the double dot is resonant with $2\omega_0$, and this absorption is made irreversible by the presence of the normal metal reservoirs. The working point $\omega_{av} = 0$ and $\Delta\omega_{LR} = Y(2\omega_0)$ corresponds to a maximal K_{loss} for $V_b = 0$ (see point (b_2)). For comparison, in the configuration of (b_1), K_{loss} is weaker because the filling of the lower dot level is less efficient. Remarkably, a nonzero V_b can be used to obtain a nonzero K_{gain} and change the relative values of K_{loss} and K_{gain} (see bottom right panel of Fig.6). For $V_b < 0$, K_{loss} increases because the filling of the lower dot level and/or the emptying of the upper dot level by the normal metal reservoirs becomes more efficient and this enhances the "reset" of the double dot between two photon pair absorption processes (Fig.6b_3). For $V_b > 0$ and sufficiently large, the filling of the upper dot level and emptying of the lower dot level are favored, which causes photon pair emission processes (see Fig.6c) while K_{loss} vanishes. In this limit, the emission of photon pair is obtained without any need for an ac cavity excitation ($\varepsilon_p = 0$) because the mesoscopic bias in V_b provides the energy for this process. The Kerr interaction K, which corresponds to the processes of Fig.6a, varies like $\mathrm{Re}[\chi_4]$ which is represented in Figs.4 and 5. Strinkingly, for $V_b = 0$, K cancels at $\Delta\omega_{LR} = Y(2\omega_0)$ where K_{loss} is maximal (see Figs.4b and 4b). Importantly, in all these plots, the order of magnitude of K_{loss}, K_{gain} and K is given by the constant $C_0 = g_L^4/\omega_0^3$. Using the typical value $\omega_0 = 2\pi \times 5$ GHz and the ratio $g_L/\omega_0 = 0.125$ which is strong but experimentally feasible, in principle (see section IV.C), one finds $C_0 = 2\pi \times 1.2$ MHz. We will see in next sections that this is be sufficient to obtain sizeable non-linear signatures in the cavity response.

2. *Average photon number*

Before studying the full quantum behavior of the cavity through the Wigner function W, it is useful to study the mean value of $\langle \hat{a} \rangle$ which can be expressed analytically. This can reveal a multistable behavior which is expected for driven nonlinear systems[44] and which will be useful to obtain photonic Schrödinger cats. From the Lindblad

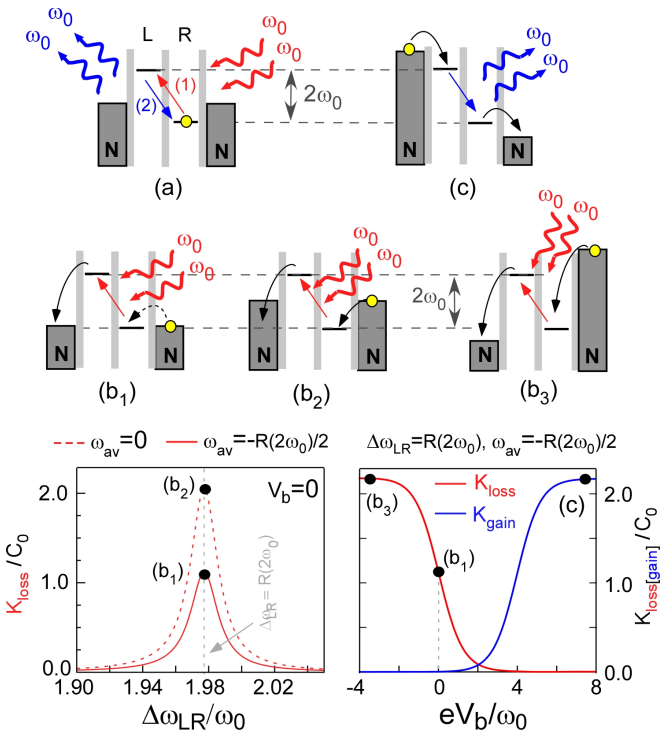

FIG. 6: Example of processes at fourth order in the light/matter coupling g. Panel (a) shows a fully coherent process which involves only the internal transition of the double dot and can contribute to the term in K. Panels (b_1), (b_2), (b_3) show processes which involve irreversible tunneling to the normal metal reservoirs and contribute to K_{loss} for different configurations of dot orbital energies and bias voltage. Panel (c) shows a process which contributes to K_{gain} in the presence of a finite bias voltage. The left bottom plot shows K_{loss} versus ω_{LR} for two difference values of ω_{av}, i.e. $\omega_{av} = R(2\omega_0)/2$ (full red line) and $\omega_{av} = 0$ (dashed red line). The right bottom plot shows K_{loss} (red full line) and K_{gain} (blue full line) versus V_b for $\omega_{av} = R(2\omega_0)/2$.

equation (46) with the fourth order terms (59) and (60) included and $\langle \hat{a} \rangle = \alpha_{av} e^{-i\omega_0 t}$, one gets

$$U_{cl}\alpha_{av}^{*} - \left(\frac{\Lambda_0 + \Delta\Lambda_{0,4}}{2} + i\chi_2 - 2i\chi_4 \left|\alpha_{av}\right|^2 \right) \alpha_{av} = 0 \tag{83}$$

with

$$\Delta\Lambda_{0,4} = \mathrm{Im}[\lambda_4 - 4(\chi_4 + U_4)] \tag{84}$$

the renormalization of the cavity linewidth to fourth order in g_L/ω_0. This Eqs. bears similarities with the result given by semiclassical approaches (see Appendix B), but the term $\Delta\Lambda_{0,4}$ is specific to a full quantum-mechanical treatment. The solution $\alpha_{av} = 0$ is obvious. However, in principle, Eq.(83) can also give nonzero values of $\alpha_{av} = \alpha_{av}^{\pm}$ given by

$$\alpha_{av}^{\pm} = \frac{1}{|\chi_4|} \sqrt{\frac{-\mathrm{Re}[\chi_2^{ren}\chi_4^{*}] \pm \sqrt{\Delta}}{2}} \tag{85}$$

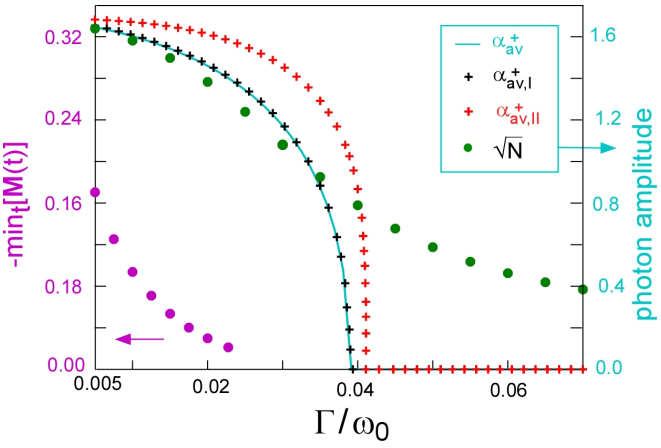

FIG. 7: Various characteristics of the cavity response versus the tunnel rate to the normal metal reservoirs Γ in the presence of the cavity drive in ε_p treated at fourth order in g_L. We use $\omega_{av} = 0.989\omega_0$, $g_L = 0.125\omega_0$ and $\Delta\omega_{LR} = R(2\omega_0) \simeq 1.978\omega_0$. The other parameters are the same as in Fig.4. The full cyan line, the black crosses and the red crosses show the semiclassical photon amplitudes α_{av}^{+} and its approximations $\alpha_{av,I}^{+}$ and $\alpha_{av,II}^{+}$ of Eqs.(85), (88) and (89), respectively. The green dots show the square root of the average photon number N in the cavity in stationnary conditions, obtained from Eq.(67). The magenta dots show the maximum negativity of the Wigner function over time t and the quadratures α, α^{*} for the protocol discussed in section IV E 3 where the cavity drive in switched on suddenly.

with

$$\Delta = |\chi_4|^2 |U_{cl}|^2 - \mathrm{Im}\left[\chi_2^{ren}\chi_4^{*}\right]^2 \tag{86}$$

and $\chi_2^{ren} = \chi_2 - i(\Lambda_0 + \Delta\Lambda_{0,4})/2$. Importantly, α_{av} must be real. Hence, from Eq.(85) for low amplitudes of β_p, the only possible solution is $\alpha_{av} = 0$ since $\Delta < 0$. For a stronger drive ($|U_{cl}| > |\mathrm{Im}\left[\chi_2^{ren}\chi_4^{*}\right]/\chi_4|$), Δ becomes positive. Then, the comparison between $\sqrt{\Delta}$ and $\pm\mathrm{Re}[\chi_4^{*}\chi_2^{ren}]$ sets whether there are 0, 1 or 2 values of α_{av} allowed by Eq.(85). Finally, two values for α_{av} are possible for each value of φ_{av}, i.e.

$$\varphi_{av}^{\pm} = -\frac{1}{2}\arg\left[\frac{i\chi_2^{ren} + 2i\chi_4 {\alpha_{av}^{\pm}}^2}{U_{cl}}\right] + n\pi \tag{87}$$

with $n \in \{0, 1\}$. In some cases, we find that α_{av}^{+} and α_{av}^{-} can be both solution to Eq. (83). However, for simplicity, we focus below on the situation of moderate interdot hopping ($t_{LR} = 0.15\omega_0$), moderate tunnel rates ($0.005\omega_0 \leq \Gamma \leq 0.1\omega_0$) and a zero bias voltage ($V_b = 0$), where one has typically a single nonzero solution α_{av}^{+}. In particular, for the parameters considered in Fig. 7, one has $|U_{cl}| \gg |U_q|$, $K = \mathrm{Re}[\chi_4] \ll -\mathrm{Im}[\chi_4]$ and $\mathrm{Im}[\chi_4] < 0$. Therefore, one has $\alpha_{av}^{+} \simeq \alpha_{av,I}^{+}$ with

$$\alpha_{av,I}^{+} = \sqrt{\frac{\mathrm{Im}[\chi_2^{ren}] + \sqrt{|U_{cl}|^2 - \mathrm{Re}\left[\chi_2^{ren}\right]^2}}{-2\,\mathrm{Im}[\chi_4]}} \tag{88}$$

This quantity is represented with black crosses in Fig.7, and is in excellent agreement with the exact α_{av}^{+} represented with a cyan line. Equation (88) shows the crucial role of the two-photon dissipation provided by the term in Im$[\chi_4]$ for the creation of nonzero photon states (if one had $|\chi_4| \to 0$, α_{av}^{+} would diverge and thus become physically irrelevant). Of course, it is also necessary to have a high enough U_{cl}. A crudest approximation is obtained by using $\chi_2^{ren} = 0$, which yields

$$\alpha_{av,II}^{+} = \sqrt{\frac{2\,|\rho_p|}{K_{loss} - K_{gain}}} \tag{89}$$

(see red crosses in Fig.7). This expression shows well that the nonzero α_{av}^{+} results from a balance between two-photon coherent injection and two-photon dissipation. In contrast, the effect of the Hamiltonian Kerr term K is negligible in Fig.7. The comparison between $\alpha_{av,I}^{+}$ and $\alpha_{av,II}^{+}$ shows that the single-photon processes described by χ_2^{ren} slightly decrease the amplitude of α_{av}^{+} and the range of Γ for which cavity bistability is obtained. Note that in principle, one has to study the stability of the $\alpha_{av}^{\pm}$ solutions to determine their relevance. We will omit such a study because the cavity Wigner function calculated in section IV E 3 can provide this information for the regime we are interested in.

3. *Cavity Wigner function to fourth order in g_L/ω_0 in non-stationary conditions*

So far, we have studied the cavity Wigner function W in stationary conditions. We now assume that the cavity is initially in the stationary vacuum state obtained in the absence of the microwave drive ($\beta_p = 0$). We want to study the time evolution of W when we switch on β_p at $t = 0$. However, since we have derived the terms in β_p in Eq.(67) in stationary conditions (see Eq.(3) and Appendix A), one has to be careful about the validity of this equation which could be jeopardized by the sudden rise of β_p. In fact, Eq. (67) will still be valid in the transient regime if we impose two constraints on the rise time of β_p. On the one hand, we will assume that this rise time is much longer that the correlation time $\sim 1/\Gamma$ associated to tunneling to the mesoscopic reservoirs, so that the terms U_{cl} and U_q in the cavity effective action can still be defined at any time from Eqs.(33) and (34) with a prefactor β_p which depends on t. On the other hand, we will assume that the rise time of β_p is much faster than the cavity characteristic evolution time (visible in Fig.8b). In these conditions, it is sufficient to use the Lindblad equation (67) with terms (59) and (60) which depend on $\beta_p(t) = \beta_p\theta(t)$ with $\theta(t)$ the Heavidside function.

We compute $W(t)$ numerically by using the function "mesolve" from the qutip package to solve Eq.(67)[56]. For moderate tunnel rates, the cavity evolves towards a coherent superposition of two coherent states (see Fig.8a).

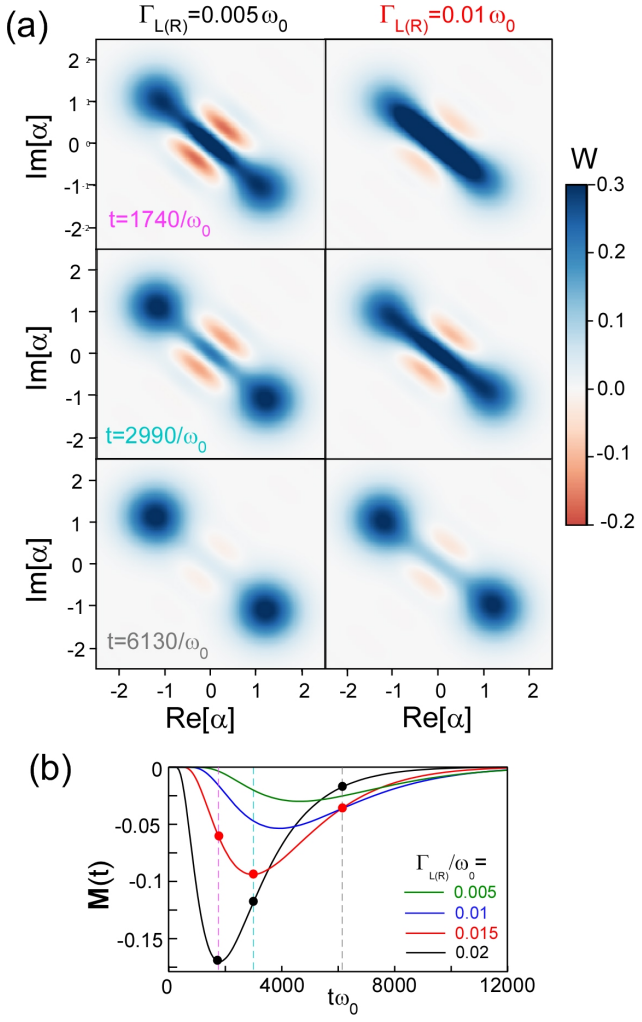

FIG. 8: Panel (a): Wigner function W of the cavity for tunnel rates $\Gamma = 0.005\omega_0$ (left panels) and $\Gamma = 0.01\omega_0$ (right panels) and different times t after switching on the cavity drive in ε_p ($t\omega_0 = 1740$, 2990, 6130 from top to bottom). The other parameters are the same as in Fig.7. Panel (b): Minimum $\mathbf{M}(t)$ of the Wigner function W over the field quadratures, versus t. The black and red points correspond to the Wigner functions in the left and right panels of (a) respectively.

The nonclassicality of $W(t)$ is revealed by the red areas where $W(t) < 0$. At large times, there remains only two positive spots in the Wigner function, which are approximately centered on the average values $\alpha_{av}^{+}e^{i\varphi_{av}^{+}}$ and $-\alpha_{av}^{+}e^{i\varphi_{av}^{+}}$ determined in section IV E 2. Therefore, these two solutions represent cavity stable states in stationary conditions. Accordingly, we have checked that the square root $\sqrt{N}$ of the average number $N = \langle \hat{a}^\dagger \hat{a} \rangle$ of photons in the cavity calculated numerically for $t \to +\infty$ matches α_{av}^{+} when the tunnel rate Γ is small (see green dots in Fig.7). For higher tunnel rates this is not the case anymore because $\alpha_{av}^{+} = 0$ whereas $W(t)$ corresponds to a squeezed vacuum.

Figure 8b represents the time evolution of the min-

imum negativity $\mathbf{M}(t) = \min_{\alpha,\alpha^*}[W(t)]$ of the Wigner function $W(t)$ over the fields quadratures (α, α^*). When Γ increases, the minimum of $\mathbf{M}(t)$ over time is reached later, which could be explained by the fact that the amplitude of the two-photon drive in ρ_p decreases (not shown). Negativities in $W(t)$ do not appear anymore if Γ is too large ($\Gamma \gtrsim 0.04\omega_0$ for the parameters of Fig.7). Figure 7 shows with magenta dots the minimum negativity $\min_t[\mathbf{M}(t)]$ of $W(t)$ over α, α^* and the time t, as a function of Γ. This quantity decreases more quickly with Γ than the amplitude of the semiclassical solution α_{av}^+. However, it is striking that a genuinely dissipative circuit such as a double quantum dot circuit is able to induce non classical cavity states thanks to the two-photon irreversible tunneling processes represented by K_{loss}. Interestingly, for $\Gamma \sim 0.01\omega_0$, the Wigner function negativity remains smaller than for $\Gamma \sim 0.005\omega_0$, but it survives longer (compare black and red curves in Fig.8). Note that in Ref.[6], a two-photon dissipation term similar to ρ_p and a two photon drive term similar to K_{loss} were obtained artificially by using an auxiliary cavity and two microwave tones. Photonic Schrödinger cats were obtained experimentally due to these effects. In our case, a single drive at $2\omega_0$ and the inclusion of a double dot in a single cavity are used to obtain these effects. For a typical cavity frequency $\omega_0 \sim 2\pi \times 5$ GHz, the required tunnel rates $\Gamma \sim 0.01\omega_0$ correspond to 0.2 μeV, a value which can be reached in practice[23,58]. With the simple protocol considered in this section, the photonic quantum superposition survives for a duration of the order of $8000/\omega_0 \simeq 0.25$ μs which is much longer than the time scale $1/\Gamma = 100/\omega_0 \simeq 3$ ns associated to dissipative tunneling between the dots and the normal reservoirs.

V. CONCLUSION

In this work, we have developed a quantum nonlinear description of mesoscopic QED experiments. More precisely, we have used a quantum path integral approach to express the effective action of a microwave cavity with bare frequency ω_0, coupled to a generic mesoscopic circuit, and excited by a microwave drive at frequency $2\omega_0$. We have developed this action to fourth order in the cavity/circuit coupling. This development reveals photon/photon interactions mediated by the mesoscopic circuit. We have investigated the possibility to establish a Markovian Lindblad description of the cavity dynamics from the cavity action. This is always possible to third order in the light matter coupling. In this limit, the cavity is subject to a coherent photon pair drive and a squeezing dissipation mediated by the mesoscopic circuit. To fourth order in the light/matter coupling, we identify particular conditions in which the Markovian approximation still holds. In this case, the mesoscopic circuit enables Kerr photon/photon interactions and two photon loss/gain stochastic processes. We have shown an example of application of our formalism to the case of a resonator coupled to a double quantum dot with normal metal contacts. We have studied how nonlinear effects such as cavity squeezing, and photonic Schrödinger cat states can occur, with a non-trivial influence of dissipative mesoscopic transport. In particular, quantum superpositions of photonic states can occur thanks to two-photon dissipation caused by tunneling processes inside the double dot circuit. The cavity squeezing effect also depends non-trivially on the dissipative tunnel rates between the dots and normal reservoirs (see Appendix F). We anticipate that the quantum regime of Mesoscopic QED conceals many more surprises which our approach can reveal. Indeed, our method can be extended straightforwardly to more complex circuit geometries with multiple quantum dots and ferromagnetic or superconducting reservoirs. The effect of Coulomb interactions inside the quantum dots also represents a rich field of investigation[59]. For simplicity, we have studied Markovian situations. However, our cavity action fully includes non-Markovian effects and it could be exploited in the non-Markovian regime by using a more general technical framework[39]. Therefore, our work should be instrumental to develop Mesoscopic QED in the quantum nonlinear regime. Interestingly, the description of the effective dynamics of microwave cavities coupled to dissipative Josephson circuits is also an important topic which lacks of systematic approaches beyond the second order in the light/matter interaction[60,61]. Our path integral approach could be used to tackle this problem.

Acknowledgements: We would like to thank Takis Kontos for illuminating discussions. ZL acknowledges support from ANR project ENDURANCE, and EMERGENCES grant ENDURANCE of Ville de Paris

Appendix A: Details on the derivation of the cavity effective action

Here, we give more details on the derivation of Eqs.(28) - (45). The drive at frequency $2\omega_0$ is not resonant with the cavity, and will affect the photonic dynamics only indirectly thanks to the nonlinearity of the mesoscopic circuit. To emphasize this fact and simplify the calculation of the cavity effective action, it is convenient to make a displacement of the cavity fields

$$\begin{bmatrix}\phi_{cl}(t)\\ \phi_q(t)\end{bmatrix} = \begin{bmatrix}\varphi_{cl}(t)\\ \varphi_q(t)\end{bmatrix} + \begin{bmatrix}\int_\omega \sqrt{2}\varepsilon_{ac}^*(\omega)\mathcal{G}_0^A(\omega)e^{i\omega t}\\ 0\end{bmatrix} \quad (90)$$

with the cavity drive ε_{ac} defined temporally in Eq.(3) and $\mathcal{G}_0^A$ the bare cavity green's function defined in Eq.(37). In this framework, the action of the system becomes

$$Z = \int d[\bar{\phi},\phi]e^{iS_{cav}^0(\bar{\phi},\phi)} \int d[\bar{\psi},\psi]e^{iS_{meso}(\bar{\varphi},\varphi,\bar{\psi},\psi)} \quad (91)$$

with S^0_{cav} defined in Eq.(19) and

$$S_{meso}(\bar{\phi},\phi,\bar{\psi},\psi) = \int\limits_{t,t'} \bar{\psi}(t)(\check{G}^{-1}(t,t') - \check{v}^{\bar{\phi},\phi}_{\Sigma}(t,t'))\psi(t') \tag{92}$$

$$\check{v}^{\bar{\phi},\phi}_{\Sigma}(t,t') = \left(\check{v}(\bar{\phi},\phi,t) + \check{v}_{ac,1}(t) + \check{v}^{\dagger}_{ac,1}(t)\right)\delta(t-t') \tag{93}$$

$$\check{v}_{ac,1}(t) = \frac{\check{g}}{2}\left(\varepsilon_p \mathcal{G}^R_0(2\omega_0)e^{-i2\omega_0 t} + \varepsilon^*_p \mathcal{G}^R_0(-2\omega_0)e^{i2\omega_0 t}\right) \tag{94}$$

In Eqs.(92)-(94), the ac drive now modifies directly the potential seen by the electrons of the mesoscopic circuit. The coefficients in $\mathcal{G}^R_0$ in Eq. (94) express how the ac drive is seen by electrons after a transduction by the cavity. They lead to the occurrence of the factor t_0 in Eq.(35).

To eliminate the electronic degrees of freedom from Eq.(91), we perform a Gaussian integration of (91) with respect to the $\bar{\psi}$ and ψ fields. This Gaussian integration is possible because, in the absence of Coulomb interactions, the system action is quadratic with respect to the electronic fields. This gives

$$Z = \int d[\bar{\phi},\phi] e^{iS^0_{cav}(\bar{\phi},\phi)}\Xi(\bar{\phi},\phi) \tag{95}$$

with

$$\Xi(\bar{\phi},\phi) = \mathcal{D}[\check{1} - \check{m}] \tag{96}$$

and

$$\check{m} = \check{G}\circ\check{v}^{\bar{\phi},\phi}_{\Sigma} \tag{97}$$

Above, $\circ$ denotes a convolution on the time variables and a matrix product on the mesoscopic orbital degrees of freedom, and $\mathcal{D}$ is a generalized determinant which can be defined as[63]

$$\begin{aligned} &Log[\Xi(\bar{\phi},\phi)] \\ &= -\int\limits_t \mathop{\mathrm{Tr}}_{k,d}\left[\check{m}(t,t) + \frac{\check{m}\circ\check{m}|_{t,t}}{2} + \frac{\check{m}\circ\check{m}\circ\check{m}|_{t,t}}{3} + ...\right] \end{aligned} \tag{98}$$

The next step is to express Eq. (98) in terms of dot Green's functions. This can generate many terms with a complex structure, but significant simplifications can be performed in the limit where the dressed cavity has a sufficient finesse. For brevity we only show the development of the second order term

$$C_2 = -\int\limits_t \mathop{\mathrm{Tr}}_{k,d}\left[\check{m}\circ\check{m}|_{t,t}/2\right]_{\varepsilon_p=0} \tag{99}$$

in Eq.(98), in the absence of the $2\omega_0$ drive ($\varepsilon_p = 0$). From the definitions of $\check{m}$ and $\check{v}^{\bar{\phi},\phi}_{\Sigma}$, one has:

$$C_2 = -\int\limits_t \mathop{\mathrm{Tr}}_{k,d}[\check{G}(t,t')\check{v}(\bar{\phi},\phi,t')\check{G}(t',t)\check{v}(\bar{\phi},\phi,t)]/4 \tag{100}$$

Using the definition (27) of $\check{v}$ in terms of fermionic fields and introducing Fourier transforms, one gets

$$\begin{aligned} C_2 = &-\iint\limits_{\omega_1,\omega_2} \mathop{\mathrm{Tr}}_{k,d}[\check{G}(\omega_1)\check{g}\bar{\phi}_{\Sigma}(\omega_3-\omega_1)\check{G}(\omega_3)\check{g}\bar{\phi}_{\Sigma}(\omega_1-\omega_3)]/4 \\ &-\iint\limits_{\omega_1,\omega_2} \mathop{\mathrm{Tr}}_{k,d}[\check{G}(\omega_1)\check{g}\bar{\phi}_{\Sigma}(\omega_3-\omega_1)\check{G}(\omega_3)\check{g}\phi_{\Sigma}(\omega_3-\omega_1)]/4 \\ &-\iint\limits_{\omega_1,\omega_2} \mathop{\mathrm{Tr}}_{k,d}[\check{G}(\omega_1)\check{g}\phi_{\Sigma}(\omega_1-\omega_3)\check{G}(\omega_3)\check{g}\bar{\phi}_{\Sigma}(\omega_1-\omega_3)]/4 \\ &-\iint\limits_{\omega_1,\omega_2} \mathop{\mathrm{Tr}}_{k,d}[\check{G}(\omega_1)\check{g}\phi_{\Sigma}(\omega_1-\omega_3)\check{G}(\omega_3)\check{g}\phi_{\Sigma}(\omega_3-\omega_1)]/4 \end{aligned} \tag{101}$$

with

$$\phi_{\Sigma}(\omega_3-\omega_1) = \phi_{cl}(\omega_3-\omega_1)\check{\sigma}_0 + \phi_q(\omega_3-\omega_1)\check{\sigma}_1 \tag{102}$$

and

$$\bar{\phi}_{\Sigma}(\omega_3-\omega_1) = \bar{\phi}_{cl}(\omega_3-\omega_1)\check{\sigma}_0 + \bar{\phi}_q(\omega_3-\omega_1)\check{\sigma}_1 \tag{103}$$

Assuming that the dressed cavity has a good quality factor ($\Lambda^{app}_0 = \Lambda_0 + \Delta\Lambda_0 \ll \omega_0$ has to be checked a posteriori), the terms $\phi_{\Sigma}(\omega_1-\omega_3)$ and $\phi_{\Sigma}(\omega_3-\omega_1)$ have a weak overlap and therefore the first and fourth line of the above expression, which contains products $\bar{\phi}_{cl(q)}\bar{\phi}_{cl[q]}$ or $\phi_{cl(q)}\phi_{cl(q)}$, are negligible. A change of frequency variables in the remaining terms (which contain contributions in $\bar{\phi}_{cl(q)}\phi_{cl[q]}$ only) gives

$$\begin{aligned} C_2 = &-\iint\limits_{\omega_1,\omega} \mathop{\mathrm{Tr}}_{k,d}[\check{G}(\omega_1)\check{g}\bar{\phi}_{\Sigma}(\omega)\check{G}(\omega+\omega_1)\check{g}\phi_{\Sigma}(\omega)]/4 \\ &-\iint\limits_{\omega_1,\omega} \mathop{\mathrm{Tr}}_{k,d}[\check{G}(\omega_1)\check{g}\phi_{\Sigma}(\omega)\check{G}(\omega_1-\omega)\check{g}\bar{\phi}_{\Sigma}(\omega)]/4 \end{aligned} \tag{104}$$

Then, we assume that the dressed cavity linewidth is much smaller than the mesoscopic resonances linewidth ($\Lambda_0 + \Delta\Lambda_0 \ll \Gamma$ has to be checked a posteriori, with Γ the order of magnitude of the tunnel rates to the mesoscopic reservoirs). In this case, the terms in $\check{G}$ in the above integral vary very slowly in the frequency area $\omega_0 - \Lambda^{app}_0 \lesssim \omega \lesssim \omega_0 + \Lambda^{app}_0$ where $\phi_{\Sigma}(\omega)$ and $\bar{\phi}_{\Sigma}(\omega)$ contribute significantly to the cavity action, and one can thus use $\omega \simeq \omega_0$ in these terms. This gives

$$\begin{aligned} C_2 = &-\iint\limits_{\omega_1,\omega} \mathop{\mathrm{Tr}}_{k,d}[\check{G}(\omega)\check{g}\bar{\phi}_{\Sigma}(\omega_1)\check{G}(\omega_0+\omega)\check{g}\phi_{\Sigma}(\omega_1)]/4 \\ &-\iint\limits_{\omega_1,\omega} \mathop{\mathrm{Tr}}_{k,d}[\check{G}(\omega)\check{g}\phi_{\Sigma}(\omega_1)\check{G}(\omega-\omega_0)\check{g}\bar{\phi}_{\Sigma}(\omega_1)]/4 \end{aligned} \tag{105}$$

Finally we can come back to the time representation for

the cavity fields

$$C_2 = -\iint_{\omega,t} \mathrm{Tr}_{k,d}[\check{G}(\omega)\check{g}\bar{\phi}_\Sigma(t)\check{G}(\omega_0+\omega)\check{g}\phi_\Sigma(t)]/4 - \iint_{\omega,\omega} \mathrm{Tr}_{k,d}[\check{G}(\omega)\check{g}\phi_\Sigma(t)\check{G}(\omega-\omega_0)\check{g}\bar{\phi}_\Sigma(t)]/4 \quad (106)$$

A rearrangement of these terms leads to an action contribution similar to that of Eq.(29), with fields $\bar{\varphi},\varphi$ replaced by $\bar{\phi}$,ϕ. A similar treatment can be performed for higher order terms of Eq.(98) and terms which depend on ε_p. For instance, the contribution in g^4 corresponds to 6 terms similar to those of Eq.(106). We finally obtain, after some algebra and term regrouping, a cavity effective Schwinger-Keldysh partition function $Z = \int d[\bar{\phi},\phi] e^{iS^{eff}_{cav}(\bar{\phi},\phi)}$ with S^{eff}_{cav} defined in Eq.(28). The final step is to come back to an expression of the cavity action with the fields $\bar{\varphi},\varphi$. We disregard terms of order $g^4\varepsilon_p$, since we assume that both g^4 and ε_p are small. In this case, one obtains $Z = \int d[\bar{\varphi},\varphi] e^{i(S^{eff}_{cav}(\bar{\varphi},\varphi)+\Delta\tilde{S}_{ac}(\bar{\varphi},\varphi))}$ where $\Delta\tilde{S}_{ac}(\bar{\varphi},\varphi)$ is a drive term similar to the term $\Delta S_{ac}(\bar{\varphi},\varphi)$ of Eq.(20), but with an amplitude ε_p which has a renormalization in $g^2\varepsilon_p$. However, since this ac drive is non resonant with the cavity, one can disregard $\Delta\tilde{S}_{ac}$. Therefore, one can use $Z \simeq \int d[\bar{\varphi},\varphi] \exp[iS^{eff}_{cav}(\bar{\varphi},\varphi)]$. In particular, one gets the expression

$$\mathcal{A} = i \begin{bmatrix} \mathcal{N}_{cl,cl,cl,cl} & \mathcal{N}_{cl,cl,cl,q} & \mathcal{N}_{cl,cl,q,q} \\ \mathcal{N}_{cl,q,cl,cl} & \mathcal{N}_{cl,q,cl,q} & \mathcal{N}_{cl,q,q,q} \\ \mathcal{N}_{q,q,cl,cl} & \mathcal{N}_{q,q,cl,q} & \mathcal{N}_{q,q,q,q} \end{bmatrix} \quad (107)$$

for the matrix which occurs in the expression (38), with coefficients $\mathcal{N}_{f,f',l,l'}$ defined in Eq.(45). Using the cyclic property of the trace in Eq.(45) and the properties $\tilde{G}_K(\omega) = -\tilde{G}_K(\omega)^\dagger$ and $\tilde{G}_a(\omega) = \tilde{G}_r(\omega)^\dagger$, one can check that there exists relations between the different components of $\mathcal{A}$ in Eq.(107) so that one finally gets expression (39).

Appendix B: Semiclassical description of Mesoscopic QED

B1. Direct semiclassical description of Mesoscopic QED

It is useful to reconsider the problem of Mesoscopic QED with a direct semiclassical approach (without the path integral formulation) in order to gain more physical insight into the new coefficients χ_4 and U_{cl} which appear in Eqs.(32) and (38). Equation (1) gives the photonic equation of motion in the Heisenberg picture:

$$\frac{d}{dt}\hat{a}(t) = -i\omega_0\hat{a}(t) - \frac{i}{\hbar}\sum_d g_d\hat{n}_d(t) - \frac{\Lambda_0}{2}\hat{a}(t) - i\varepsilon_{ac}(t) \quad (108)$$

In a semiclassical picture, the operator $\hat{a}(t)$ in the above equation can be treated as a classical quantity $a(t) = \hat{a}(t) = \langle\hat{a}(t)\rangle$. In this case, the average electron number operator $\langle\hat{n}_d(t)\rangle = \left\langle \hat{c}^\dagger_d(t)\hat{c}_d(t)\right\rangle$ in orbital d can be calculated as the response to the "classical" excitations $g_{d'}(a^\dagger(t)+a(t))$, with $d' \in [1,N]$, which we will write in a matrix form as

$$\tilde{E}_{ac}(t) = \tilde{g}(a^\dagger(t)+a(t)) \quad (109)$$

At this stage, although $a(t)$ is expected to have a dominant contribution in $e^{-i\omega_0 t}$, it is essential to take into account weak components in $e^{\pm i2\omega_0 t}$ to describe the effect of the drive in β_p on $\langle\hat{n}_d(t)\rangle$. It is sufficient to estimate these components from Eq.(108) treated to order 0 in $\tilde{g}$, because this is enough to obtain a $\beta_p\tilde{g}^3$ contribution to the photonic field, as we will see below. Hence, we use

$$\tilde{E}_{ac}(t) = \tilde{g}\left(\alpha e^{-i\omega_0 t} + \alpha^* e^{i\omega_0 t} + \mathrm{Re}[t_0\varepsilon_p e^{-i2\omega_0 t}/2]\right) \quad (110)$$

with t_0 defined by Eq.(36). The amplitude α is not specified since it must be determined self-consistently from Eq.(108) and the response of the average dot charges to $\tilde{E}_{ac}(t)$. From the Keldysh description of mesoscopic transport[52], this response is given by

$$\sum_d g_d\langle\hat{n}_d(t)\rangle = -iTr_d[\tilde{g}\tilde{\mathbf{G}}_<(t,t)] \quad (111)$$

where the lesser Green's function of the dots $\tilde{\mathbf{G}}_<$ in the presence of $\tilde{E}_{ac}(t)$ can be expressed as

$$\tilde{\mathbf{G}}_<(t,t) = \iiint \frac{d\omega}{2\pi} dt_1 dt_2 e^{-i\omega(t_1-t_2)}\tilde{\mathbf{G}}_r(t,t_1)\tilde{\Sigma}^<(\omega)\tilde{\mathbf{G}}_a(t_2,t) \quad (112)$$

Above, $\tilde{\Sigma}^<(\omega)$ is the lesser self energy of the dots illustrated in section IV B for the double dot case. The mesoscopic retarded and advanced Green's functions $\tilde{\mathbf{G}}_{r(a)}$ in the presence of $\tilde{E}_{ac}(t)$ can be calculated in terms of the unperturbed mesoscopic Green's functions $\tilde{G}_{r(a)}$ defined in section III A by using the Dyson equation

$$\tilde{\mathbf{G}}_J(t,t') = \tilde{G}_J(t,t') + \int \frac{dt_1}{\hbar}\tilde{G}_J(t,t_1)\tilde{E}_{ac}(t_1)\tilde{\mathbf{G}}_J(t_1,t') \quad (113)$$

with $J \in r(a)$.

The combination of Eqs.(111), (112) and (113) gives, by keeping only resonant contributions in $e^{-i\omega_0 t}$,

$$\sum_d g_d\langle\hat{n}_d\rangle \simeq \left(\alpha\chi_2 + 2\alpha|\alpha|^2\chi_4 + i\alpha^* U_{cl}\right)e^{-i\omega_0 t} \quad (114)$$

Tedious algebra is necessary to identify the coefficients which appear in Eq.(114) with the correlation functions U_{cl} and χ_4 defined in the main text, especially in the multi-orbital case $N > 1$. Equation (114) shows that χ_2 is the linear response function of the dots charge to the excitation in $\alpha e^{-i\omega_0 t}$, and χ_4 is the second order response

function to the same excitation, whereas U_{cl} appears as a transduction coefficient for the field component in $\alpha^* e^{i\omega_0 t}$ into a resonant term in $e^{-i\omega_0 t}$ thanks to the energy provided by the drive in ε_p. One can finally inject Eq.(114) into the statistical average of Eq.(108) to obtain

$$0 = \alpha^* U_{cl} - \left(i\chi_2 + \frac{\Lambda_0}{2} - 2i\left|\alpha\right|^2 \chi_4 \right) \alpha \qquad (115)$$

For this last step, we have used the resonant approximation $\varepsilon_{ac}(t) \simeq \varepsilon e^{-i\omega_0 t}$ in Eq.(108). One can see along this calculation that ε_p plays a crucial role in intermediary steps of the calculation for the description of two photon processes, but its direct resonant contribution to (115) can be disregarded. A similar fact happens with the path integral approach where ε_p produces indirectly the $S_g^{(3)}(t)$ term whereas its direct contribution $\Delta S_{ac}(t)$ can be disregarded from the effective action $S_{cav}^{eff}(t)$ in the resonant approximation. Note that Eq.(115) is in full agreement with the result given by a direct calculation of the semiclassical cavity steady states with the path integral description (see Appendix B2).

B2. Semiclassical photonic amplitudes given by the path integral description

The possible semiclassical photonic amplitudes of the cavity in stationary conditions can also be obtained by looking for the saddle points of the cavity effective action[39]. Since the action (28) vanishes for $\varphi_{cl} = 0$, $\bar{\varphi}_{cl} = 0$, a semiclassical solution for the cavity field can be found at $\varphi_q = 0$, $\bar{\varphi}_q = 0$ and values of φ_{cl} and $\bar{\varphi}_{cl}$ such that $\partial(S)/\partial\bar{\varphi}_q(t)|_{\varphi_q=0,\bar{\varphi}_q=0} = 0$. This gives

$$\begin{aligned} -\sqrt{2}\varepsilon_{ac}(t) = (i\partial_t - \omega_0 + \frac{i\Lambda_0}{2})\varphi_{cl} - \chi_2\varphi_{cl} \qquad (116) \\ - ie^{-2i\omega_0 t} U_{cl}\bar{\varphi}_{cl} - \chi_4\bar{\varphi}_{cl}\varphi_{cl}\varphi_{cl} \end{aligned}$$

One can disregarded $\varepsilon_{ac}(t)$ from the left member of Eq. (116) because it is not directly resonant with the cavity. Hence, one can expect a semiclassical solution $\varphi_{sc} = \sqrt{2}\alpha_{sc} e^{i(\varphi_{sc} - \omega_0 t)}$ such that

$$\left(U_{cl} e^{-2i\varphi_{sc}} - \frac{\Lambda_0}{2} - i\chi_2 - 2i\chi_4 \left|\alpha_{sc}\right|^2 \right) \alpha_{sc} = 0 \qquad (117)$$

with α_{sc} the semiclassical value of $\hat{a}$. Equation (117) is in full agreement with the semiclassical Eq. (115) if $\alpha = \alpha_{sc}$ is used. This equation is also similar to the equation (83) on the average photons amplitude α_{av} obtained from the Lindblad description of the cavity dynamics, up to the term in $\Delta\Lambda_{0,4}$ which is not present in Eq.(117). This discrepancy is due to the fact that the equation on α_{sc} is obtained by disregarding quantum fluctuations of the cavity occupation.

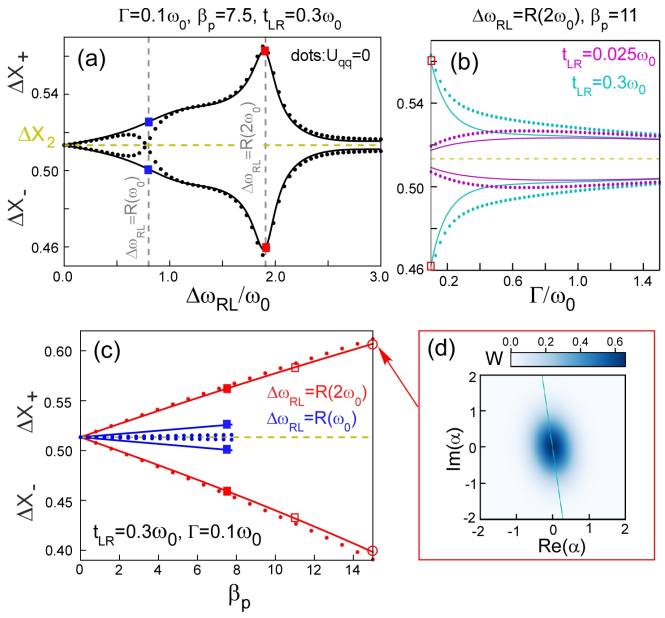

FIG. 9: Panels (a), (b) and (c): Cavity field quadratures $\Delta X_\pm$ versus $\Delta\omega_{RL}$, Γ and β_p respectively. In panel (a), we use $t_{LR} = 0.3\omega_0$, $\Gamma = 0.1\omega_0$ and $\beta_p = 7.5$. In panel (b) we use $t_{LR} = 0.3\omega_0$ (cyan lines) or $t_{LR} = 0.025\omega_0$ (magenta lines), $\Delta\omega_{RL} = R(2\omega_0)$ and $\beta_p = 11$. In panel (c) we use $t_{LR} = 0.3$, $\Gamma = 0.1\omega_0$ and $\Delta\omega_{RL} = R(2\omega_0)$ (red lines) or $\Delta\omega_{RL} = R(\omega_0)$ (blue lines). The other parameters are the same as in Fig. 3 with $\omega_{av} = 0$ and $g_L = 0.01\omega_0$. The full lines correspond to the result given by the full expressions (81) and (82) of A and B whereas the dotted lines omit the contribution of γ_p (or equivalently U_{qq}). For reference, the second order variance ΔX_2 for an empty cavity (corresponding to the case for $g_L = 0$) is also shown as a dashed yellow line. The vertical dashed gray lines in panel (a) indicate the resonances $\Delta\omega_{RL} = R(\omega_0)$ and $\Delta\omega_{RL} = R(2\omega_0)$. The blue and red squares indicate working points which are common to panels (a), (b) and (c). In panel (c), the plots are restricted to the range where $\gamma_{loss} > 0$ and $\gamma_{gain} > 0$, which is narrower in the case $\Delta\omega_{RL} = R(\omega_0)$ (blue curves). Panel d: Squeezed cavity Wigner function for the working point corresponding to the empty red circles in panel (c). The major axis of the Wigner function is shown as a blue line.

Appendix C:Action associated to a master equation description

Following Ref.[62], the action corresponding to the master equation with the form (46) can be expressed as

$$S = \int_t (\bar{\varphi}_+(t) i\partial t\varphi_+(t) - \bar{\varphi}_-(t) i\partial t\varphi_-(t) - i\mathcal{L}(t) \qquad (118)$$

with $\varphi_\pm = \frac{1}{\sqrt{2}}(\varphi_{cl} \pm \varphi_q)$, $\bar{\varphi}_\pm = \frac{1}{\sqrt{2}}(\bar{\varphi}_{cl} \pm \bar{\varphi}_q)$ and

$$\begin{aligned} -i\mathcal{L}(t) = &-H^{eff}_{cav}[\bar{\varphi}_+(t), \varphi_+(t)] + H^{eff}_{cav}[\bar{\varphi}_-(t), \varphi_-(t)] \\ &- i\sum_j \gamma_j \hat{L}_j[\bar{\varphi}_+, \varphi_+]\hat{L}^\dagger_j[\bar{\varphi}_-, \varphi_-] \\ &+ \frac{i}{2}\sum_{j,s\in\{+,-\}} \gamma_j \hat{L}^\dagger_j[\bar{\varphi}_s, \varphi_s]\hat{L}_j[\bar{\varphi}_s, \varphi_s] \end{aligned} \tag{119}$$

This leads to Eqs.(49), (61), and (62) of the main text. Note that this result is valid even when the dissipative rates γ_j and the Hamiltonian H^{eff}_{cav} are time-dependent

Appendix D: Link between the direct density matrix approach and the path integral approach to second order in $\check{g}$

To show that the Lindblad Eqs.(12) and (67) obtained with the direct density matrix approach and the path integral approach, respectively, agree to second order in $\check{g}$, one must establish the relation between the parameters χ_A, χ_B and χ_2, λ_2 which occur in these Eqs. Note that χ_2 and λ_2 have a frequency dependence which is omitted in the main text where we use $\chi_2 = \chi_2(\omega_0)$, and $\lambda_2 = \lambda_2(\omega_0)$. For our present purpose, it is convenient to use the inverse Fourier transform of these quantities, defined generally as $f(t) = \int_{-\infty}^{+\infty} \frac{d\omega_0}{2\pi} f(\omega_0)e^{-i\omega_0 t}$. One can use the general relation

$$\int_{-\infty}^{+\infty} \frac{d\omega}{2\pi} a(\omega+\omega_0)b(\omega) = \int_{-\infty}^{+\infty} dt\ a(t)b(-t)e^{i\omega_0 t} \tag{120}$$

where a and b are two generic functions, to reexpress Eqs.(30) and (31) as

$$\chi_2(t) = -\frac{i}{2}\underset{d}{\mathrm{Tr}}\left[\tilde{G}_K(t)\tilde{g}\tilde{G}_a(-t)\tilde{g} + \tilde{G}_K(-t)\tilde{g}\tilde{G}_r(t)\tilde{g}\right] \tag{121}$$

$$\begin{aligned} \lambda_2(t) = -\frac{i}{2}\underset{d}{\mathrm{Tr}}\Big[&\tilde{G}_K(-t)\tilde{g}\tilde{G}_K(t)\tilde{g} \\ &+ \tilde{G}_a(-t)\tilde{g}\tilde{G}_r(t)\tilde{g} + \tilde{G}_r(-t)\tilde{g}\tilde{G}_a(t)\tilde{g}\Big] \end{aligned} \tag{122}$$

At this stage, it is convenient to define the lesser and greater fermionic Green's functions

$$G^{d,d'}_<(t) = i\left\langle \hat{c}^\dagger_{d'}(0)\hat{c}_d(t)\right\rangle \tag{123}$$

$$G^{d,d'}_>(t) = -i\left\langle \hat{c}_d(t)\hat{c}^\dagger_{d'}(0)\right\rangle \tag{124}$$

to reexpress definitions (24)-(26) as:

$$G^{d,d'}_r(t) = \theta(t)\left(G^{d,d'}_>(t) - G^{d,d'}_<(t)\right) \tag{125}$$

$$G^{d,d'}_a(t) = \theta(-t)\left(G^{d,d'}_<(t) - G^{d,d'}_>(t)\right) \tag{126}$$

and

$$G^{d,d'}_K(t) = G^{d,d'}_<(t) + G^{d,d'}_>(t) \tag{127}$$

Then, using Eqs.(125)-(127), one can rewrite Eqs.(121) and (122) as

$$\chi_2(t) = i\theta(t)\underset{d}{\mathrm{Tr}}\left[\tilde{G}_<(t)\tilde{g}\tilde{G}_>(-t)\tilde{g} - \tilde{G}_>(t)\tilde{g}\tilde{G}_<(-t)\tilde{g}\right] \tag{128}$$

$$\lambda_2(t) = -i\underset{d}{\mathrm{Tr}}\left[\tilde{G}_<(-t)\tilde{g}\tilde{G}_>(t)\tilde{g} + \tilde{G}_>(-t)\tilde{g}\tilde{G}_<(t)\tilde{g}\right] \tag{129}$$

Since we consider a non-interacting case, one can use the Wick theorem to reexpress the above equations in terms of charge correlators[47]. Indeed, using the operator $\hat{N}(t)$ of Eq. (6), one finds

$$\left\langle \hat{N}(t)\hat{N}(0)\right\rangle = \left\langle \hat{N}\right\rangle^2 + \underset{d}{\mathrm{Tr}}\left[\tilde{G}_<(-t)\tilde{g}\tilde{G}_>(t)\tilde{g}\right] \tag{130}$$

$$\left\langle \hat{N}(0)\hat{N}(t)\right\rangle = \left\langle \hat{N}\right\rangle^2 + \underset{d}{\mathrm{Tr}}\left[\tilde{G}_<(t)\tilde{g}\tilde{G}_>(-t)\tilde{g}\right] \tag{131}$$

This leads to

$$\chi_2(t) = i\theta(t)\left(\left\langle \hat{N}(0)\hat{N}(t)\right\rangle - \left\langle \hat{N}(t)\hat{N}(0)\right\rangle\right) \tag{132}$$

$$\lambda_2(t) = -i\left(\left\langle \hat{N}(0)\hat{N}(t)\right\rangle + \left\langle \hat{N}(t)\hat{N}(0)\right\rangle - 2\left\langle \hat{N}\right\rangle^2\right) \tag{133}$$

A comparison of these equations with the definitions (14) and (15) of $\chi_A(t)$ and $\chi_B(t)$ gives, in the frequency domain

$$\chi_2(\omega_0) = \chi_B(\omega_0) - \chi_A(\omega_0) \tag{134}$$

$$\lambda_2(\omega_0) = 2i\left(\mathrm{Im}[\chi_A(\omega_0) + \chi_B(\omega_0)] + \left\langle \hat{N}\right\rangle^2 \delta(\omega_0)\right) \tag{135}$$

This proves the relations (70) and (71) of the main text and the agreement between the Lindblad Eqs.(12) and (67) at second order in $\check{g}/\omega_0$.

Appendix E: Analytical calculation of the Wigner function to third order in $\check{g}/\omega_0$

The definition (77) of the Wigner function involves the correlation function $\chi(t,\beta,\beta^*) = \left\langle e^{\beta a^\dagger_I - \beta^* a_I}\right\rangle_t$. From the expression of the effective Hamiltonian H^{eff}_{cav} and the jump operators $\hat{L}_j$, one can check that χ follows[39]

$$\begin{aligned} \frac{\partial}{\partial t}\chi = &-i\Delta\omega_0\left(-\beta\partial_\beta + \beta^*\partial_{\beta^*}\right)\chi - \gamma_+\frac{\beta\beta^*}{2}\chi \\ &- \frac{\gamma_-}{2}\left(\beta^*\partial_{\beta^*} + \beta\partial_\beta\right)\chi - 2\rho_p\beta^*\partial_\beta\chi - 2\rho^*_p\beta\partial_{\beta^*}\chi \\ &- \frac{\beta^2}{2}\gamma_p e^{-i\varphi_p}\chi - \frac{\beta^{*2}}{2}\gamma_p e^{i\varphi_p}\chi \end{aligned} \tag{136}$$

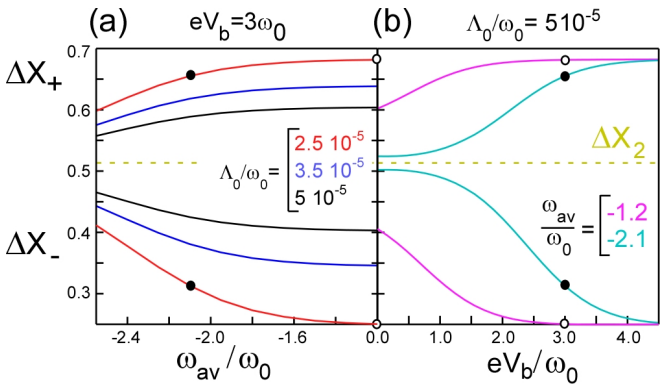

FIG. 10: Cavity field quadratures $\Delta X_\pm$ versus $\omega_{av} = (\omega_R + \omega_L)/2$ (panel (a)) and versus the bias voltage V_b (panel (b)) for $\Delta\omega_{RL} = 2\omega_0$, $t_{LR} = 0.1\omega_0$, $g_L = 0.01\omega_0$ and $\beta_p = 200$. The other parameters are the same as in Fig.3. Panel (a) considers different cavity damping rates $\Lambda_0/(10^{-5}\omega_0) = 2.5$, 3.5 and 5 with red, blue and black lines. Panel (b) shows results for average dot orbital energies $\omega_{av}/\omega_0 = -2.1$ (cyan lines) and $\omega_{av}/\omega_0 = -1.2$ (green lines). The circles indicate working points common to panels (a) and (b). For reference, the second order variance $\Delta X_2 = \sqrt{1+2n_B}/2$ for a decoupled cavity ($g_L = 0$) is also shown as a dashed yellow line. It is independent of the value of Λ_0.

For compactness we note $\frac{\partial}{\partial\beta} = \partial_\beta$ and $\frac{\partial}{\partial\beta^*} = \partial_{\beta^*}$. The above equation is a first order differential equation which is more convenient to solve than the second order differential equation (77). It is then straightforward to Fourier transform χ to obtain $W(t)$.

Appendix F: Parametric control of the squeezing effect

This Appendix discusses how the photonic squeezing effect of Section IV.D depends on the double dot parameters. Figure 9 shows the cavity field quadratures $\Delta X_\pm$ versus the orbital detuning $\Delta\omega_{RL} = \omega_R - \omega_L$ (panel (a)), versus Γ (panel (b)) and versus the cavity drive amplitude β_p (panel (c)) for a case where the single and two photon resonances at $\Delta\omega_{RL} = Y(\omega_0)$ and $\Delta\omega_{RL} = Y(2\omega_0)$ are allowed. The results given by the full expressions (81) and (82) of A and B are shown with full lines. For reference, the variance

$$\Delta X_2 = \frac{1}{2}\sqrt{\frac{\Lambda_0(1+2n_B) - \mathrm{Im}[\lambda_2]}{\Lambda_0 - 2\,\mathrm{Im}[\chi_2]}} \qquad (137)$$

of the cavity field to second order in g_L is also shown as a yellow line. One gets a squeezing effect ($\Delta X_- < \Delta X_2 < \Delta X_+$) which is maximal at $\Delta\omega_{RL} = Y(2\omega_0)$ (panel (a)). As visible in panel (b), for $t_{LR} = 0.3$ (cyan full line), squeezing decreases with Γ. One could expect that higher values of Γ are always detrimental to squeezing. However, for a small value of t_{LR} (magenta full lines), the squeezing effect finds a local maximum for a value of Γ which can be quite significant ($\Gamma \sim 0.9\omega_0$ in panel (b)).

To determine the role of the parameter U_q (or γ_p), we show with dotted lines in Fig. 9a, b and c, the cavity field quadratures given by Eqs. (81) and (82) with γ_p omitted ($\gamma_p = 0$). For the moderate tunnel rate Γ used in panel (a), the full and dotted lines coincide around $\Delta\omega_{RL} = Y(2\omega_0)$ but not near the single photon resonance $\Delta\omega_{RL} = Y(\omega_0)$. Surprisingly, for $\Delta\omega_{RL} = Y(\omega_0)$, the dissipative term in U_q is responsible for an increase of the squeezing effect, in spite of its dissipative nature. Such an effect is allowed by Eq.(82). To see an effect of U_q on the squeezing at the working point $\Delta\omega_{RL} = Y(2\omega_0)$, it is necessary to increase the value of Γ (see panel (b)). In this case, U_q causes a decrease of the squeezing amplitude. To summarize, the dissipative term in U_q can either increase or decrease the squeezing effect, depending on the regime of parameters. Nevertheless, to maximize the squeezing effect, it is advantageous to use the regime $\Delta\omega_{RL} = Y(2\omega_0)$ and Γ small, where the effect of U_q can be disregarded (empty red squares in Fig.9b). Therefore we will consider this regime in the rest of the present Appendix and Fig.10.

The use of a double quantum dot circuit as a nonlinear element for circuit QED can be interesting because it offers a strong tunability of the squeezing effect, as already seen in Fig.9. Figure 10a shows that the amplitude of the squeezing effect is also strongly dependent on the average level position $\omega_{av} = (\omega_L + \omega_R)/2$. Besides, the squeezing effect can be controlled by using a nonzero bias voltage V_b (see Fig.10b). This is consistent with the fact mentioned earlier that using a nonzero V_b modifies the orbital energy range where the drive terms U_{cl} shows strong resonances (Fig.3a and c). Note that, so far, we have used a relatively high cavity damping rate Λ_0 which limits the squeezing effect. Panels (a) and (b) of Fig. 10 show that for a given set of double dot parameters, the squeezing effect increases when Λ_0 decreases, as expected. Finally, Fig. 9c shows an example of cavity Wigner function corresponding to the red empty circles in Fig.9. Using the qutip package mesolve[56], we have checked that this Wigner function is in quantitative agreement with a direct numerical treatment of Eq. (46). We have also checked that fourth order corrections in g_L are negligible for the parameters considered in the present section. Therefore, a treatment of the master equation (46) to third order in g_L is fully justified for the parameters used in section IV D.

Interestingly, it has also been suggested to obtain cavity squeezing by using a single quantum dot with an ac excitation with amplitude ε'_p applied directly to the dot gate[57]. However, on the experimental level, such a strategy is more costly since it requires to fabricate a direct ac gate for the quantum dot. Note that Ref.[57] presents the cavity effective action to second order in g_L only. A coherent two-photon drive term in $\varepsilon'_p g_L^2$ is taken into account but the terms in χ_2, λ_2 and the expected contribution in $\varepsilon'_p g_L^2$ to U_q are disregarded. Alternatively, two-

photon processes or photonic squeezing have been found for dc voltage-biased Josephson junctions or tunnel junctions, which have no internal degrees of freedom[64–68]. In our case, the dc voltage-bias is not necessary due to the presence of the dot orbital degree of freedom.

[1] A. Wallraff et al., *Strong coupling of a single photon to a superconducting qubit using circuit quantum electrodynamics*, Nature **431**, 162 (2004).

[2] F. Mallet et al., *Quantum state tomography of an itinerant squeezed microwave field*, Phys. Rev. Lett. **106**, 220502 (2011).

[3] G. Kirchmair et al., *Observation of quantum state collapse and revival due to the single-photon Kerr effect*, Nature **495**, 205 (2013).

[4] M. Hofheinz et al. *Generation of Fock states in a superconducting quantum circuit*, Nature **454**, 310 (2008).

[5] M. Hofheinz et al. *Synthesizing arbitrary quantum states in a superconducting resonator*, Nature **459**, 546 (2009).

[6] Z. Leghtas et al., *Confining the state of light to a quantum manifold by engineered two-photon loss*, Science, **347**, 853 (2015).

[7] E. T. Holland et al., *Single-photon Resolved Cross-Kerr Interaction for Autonomous Stabilization of Photon-number States*, Phys. Rev. Lett. **115**, 180501 (2015).

[8] J. F. Poyatos, J. I. Cirac, and P. Zoller, *Quantum Reservoir Engineering with Laser Cooled Trapped Ions*, Phys. Rev. Lett. **77**, 4728 (1996).

[9] A. Sarlette, Z. Leghtas, M. Brune, J. M. Raimond, and P. Rouchon, *Stabilization of nonclassical states of one- and two-mode radiation fields by reservoir engineering*, Phys. Rev. A **86**, 012114 (2012).

[10] C. Aron, M. Kulkarni, and H. E. Türeci, *Steady-state entanglement of spatially separated qubits via quantum bath engineering*, Phys. Rev. A **90**, 062305 (2014).

[11] A. Roy et al., *Continuous Generation and Stabilization of Mesoscopic Field Superposition States in a Quantum Circuit*, Phys. Rev. A **91**, 013810 (2015).

[12] C. M. Caves, K. S. Thorne, R. W. P. Drever, V. D. Sandberg, and M. Zimmermann. *On the measurement of a weak classical force coupled to a quantum-mechanical oscillator*, Rev. Mod. Phys. **52**, 341 (1980).

[13] V. Giovannetti, S. Lloyd and L. Maccone, *Quantum-Enhanced Measurements: Beating the Standard Quantum Limit*, Science **306**, 1330 (2004).

[14] M. Mirrahimi et al., *Dynamically protected cat-qubits: a new paradigm for universal quantum computation*, New J. Phys. **16**, 045014 (2014).

[15] S. Haroche and J.-M.Raimond, *Exploring the Quantum: Atoms, Cavities, and Photons*, Oxford Graduate Texts (2006).

[16] B. Reulet, M. Ramin, H. Bouchiat, and D. Mailly, *Dynamic response of isolated Aharonov-Bohm rings coupled to an electromagnetic resonator*, Phys. Rev. Lett. **75**, 124 (1995).

[17] A. Cottet et al., *Cavity QED with hybrid nanocircuits: from atomic-like physics to condensed matter phenomena,* J. Phys.: Condens. Matter **29**, 433002 (2017).

[18] M. R. Delbecq et al., *Coupling a quantum dot, fermionic leads and a microwave cavity on-chip*, Phys. Rev. Lett. **107**, 256804 (2011).

[19] T. Frey et al., *Dipole Coupling of a Double Quantum Dot to a Microwave Resonator*, Phys. Rev. Lett. **108** 046807 (2012).

[20] J.J. Viennot, M.C. Dartiailh, A. Cottet, and T. Kontos, *Coherent coupling of a single spin to microwave cavity photons*, Science **349**, 408 (2015).

[21] T. Cubaynes, M. R. Delbecq, M. C. Dartiailh, R. Assouly, M. M. Desjardins, L. C. Contamin, L. E. Bruhat, Z. Leghtas, F. Mallet, A. Cottet, T. Kontos, *Highly coherent spin states in carbon nanotubes coupled to cavity photons*, npj Quantum Information **5**, Article number: 47 (2019).

[22] L. E. Bruhat, T. Cubaynes, J J. Viennot, M. C. Dartiailh, M. M. Desjardins, A. Cottet and T. Kontos, *Cavity photons as a probe for charge relaxation resistance and photon emission in a quantum dot coupled to normal and superconducting continua*, Phys. Rev. X **6**, 021014 (2016).

[23] L.E. Bruhat, T. Cubaynes, J.J. Viennot et al., *Circuit QED with a quantum-dot charge qubit dressed by Cooper pairs*, Phys. Rev. B **98**, 155313 (2018).

[24] X. Mi, J. V. Cady, D. M. Zajac, P. W. Deelman, J. R. Petta, *Strong Coupling of a Single Electron in Silicon to a Microwave Photon*, Science **355**, 156 (2017).

[25] A. Stockklauser, P. Scarlino, J.-V. Koski et al. *Strong Coupling Cavity QED with Gate-Defined Double Quantum Dots*, Phys. Rev. X **7**, 011030 (2017).

[26] X. Mi, M. Benito, S. Putz, D. M. Zajac, J. M. Taylor, G. Burkard, and J. R. Petta, *A coherent spin–photon interface in silicon*, Nature **555**, 599 (2018).

[27] N. Samkharadze et al., *Strong spin-photon coupling in silicon*, Science **359**, 1123 (2018).

[28] A. J. Landig et al., *Coherent spin-qubit photon coupling*, Nature **560**, 179-184 (2018).

[29] M. Schiró and K. Le Hur, *Tunable hybrid quantum electrodynamics from nonlinear electron transport*, Phys. Rev. B **89** 195127 (2014).

[30] O Dmytruk, M Trif and P Simon, *Cavity quantum electrodynamics with mesoscopic topological superconductors*, Phys. Rev. B **92** 245432 (2015).

[31] O. Dmytruk, M. Trif, C. Mora, P.Simon, *Cavity quantum electrodynamics with an out-of-equilibrium quantum dot*, Phys. Rev. B **93**, 075425 (2016).

[32] M.C. Dartiailh, T. Kontos, B. Douçot, and A. Cottet, *Direct cavity detection of Majorana pairs*, Phys. Rev. Lett. **118**, 126803 (2017).

[33] P.-Q. Jin, M.Marthaler, J. H. Cole, A. Shnirman, and G. Schön, *Lasing and transport in a quantum-dot resonator circuit*, Phys. Rev. B **84**, 035322 (2011).

[34] P.-Q. Jin, M. Marthaler, J. H. Cole, A. Shnirman and G. Schön, *Lasing and transport in a coupled quantum dot-resonator system*, Phys. Scr. **T151**, 014032 (2012).

[35] P.-Q. Jin, M. Marthaler, P.-Q. Jin, D. Golubev and G. Schön, *Noise spectrum of a quantum dot-resonator lasing circuit*, New Journal of Physics **15**, 025044 (2013).

[36] M. Kulkarni, O. Cotlet, H. E. Türeci, *Cavity-coupled double-quantum dot at finite bias: analogy with lasers and beyond,* Phys. Rev. B **90**, 125402 (2014).

[37] A. Stockklauser, V. F. Maisi, J. Basset, K. Cujia, C. Reichl, W. Wegscheider, T. Ihn, A. Wallraff, and K. Ensslin,

Microwave Emission from Hybridized States in a Semiconductor Charge Qubit, Phys.Rev. Lett. **115**, 046802 (2015).

[38] J.J. Viennot, M.R. Delbecq, M.C. Dartiailh, A. Cottet, T. Kontos, *Out of equilibrium charge dynamics in a hybrid cQED architecture*, Phys. Rev. B **89**, 165404 (2014).

[39] A. Kamenev, *Field Theory of Non-Equilibrium Systems*, Cambridge University Press (2011).

[40] M. Trif and Y. Tserkovnyak, *Resonantly Tunable Majorana Polariton in a Microwave Cavity*, Phys. Rev. Lett. **109** 257002 (2012).

[41] T L Schmidt, A Nunnenkamp and C Bruder, *Majorana Qubit Rotations in Microwave Cavities*, Phys. Rev. Lett. **110** 107006 (2013).

[42] A Cottet, T Kontos and B Douçot, *Squeezing light with Majorana fermions*, Phys. Rev. B **88** 195415 (2013).

[43] A. Cottet, T. Kontos and B. Douçot, *Electron-photon coupling in Mesoscopic Quantum Electrodynamics*, Phys. Rev. B **91**, 205417 (2015).

[44] Walls D F Milburn G J 2008 *Quantum Optics*, 2nd edn. Springer, Berlin

[45] M. Benito et al., *Input-output theory for spin-photon coupling in Si double quantum dots,* Phys. Rev. B **96**, 235434 (2017).

[46] K. Blum, *Density matrix theory and applications*, third edition, Springer (2012).

[47] R. Zamoum, M. Lavagna, and A. Crépieux, *Nonsymmetrized noise in a quantum dot: Interpretation in terms of energy transfer and coherent superposition of scattering paths*, Phys. Rev. B **93**, 235449 (2016).

[48] More mathematically speaking, $\varphi_\pm(t)$ and $\psi_{\pm,d}(t)$ represent eigenvalues of the operators $\hat{a}$ and $\hat{c}_d$ in a coherent eigenstates picture where one can use $\hat{a}\,|\varphi_\pm(t)\rangle = \varphi_\pm(t)\,|\varphi_\pm(t)\rangle$ and $\hat{c}_d\,|\psi_{\pm,d}(t)\rangle = \psi_{\pm,d}(t)\,|\psi_{\pm,d}(t)\rangle$. Details on the contruction of this representation are given in Refs.[39,63].

[49] E. G. Dalla Torre, S. Diehl, M. D. Lukin, S. Sachdev, and P. Strack, *Keldysh approach for nonequilibrium phase transitions in quantum optics: Beyond the Dicke model in optical cavities*, Phys. Rev. A **87**, 023831 (2013).

[50] A. Cottet, C. Mora and T. Kontos, *Mesoscopic admittance of a double quantum dot*, Phys. Rev. B **83**, 121311(R) (2011).

[51] This is possible provided the capacitances to the source and drain contacts are equal and the capacitance between the two dots is very large. In the general case, our results will remain valid provided $\omega_{L(R)}$ are understood as V-shifted orbital energies.

[52] A.-P. Jauho, N. S. Wingreen, and Y. Meir, *Time-Dependent Transport in Interacting and Noninteracting Resonant-Tunneling Systems*, Phys. Rev. B **50**, 5528 (1994).

[53] V. Talbo, M. Lavagna, T. Q. Duong, and A. Crépieux, *Charge susceptibility and conductances of a double quantum dot*, AIP Advances **8**, 101333 (2018).

[54] N. Samkharadze et al., *Strong spin-photon coupling in silicon,* Science **359**, 1123 (2018).

[55] N. Samkharadze, A. Bruno, P. Scarlino, G. Zheng, D. P. DiVincenzo, L. DiCarlo, and L. M. K. Vandersypen, *High-Kinetic-Inductance Superconducting Nanowire Resonators for Circuit QED in a Magnetic Field*, Phys. Rev. Applied **5**, 044004 (2016).

[56] J. R. Johansson, P. D. Nation, and F. Nori: "*QuTiP: An open-source Python framework for the dynamics of open quantum systems*", Comp. Phys. Comm. **183**, 1760–1772 (2012).

[57] U. C. Mendes and C. Mora, *Cavity squeezing by a quantum conductor*, New J. Phys. **17**, 113014 (2015).

[58] S. Gustavsson et al., *Counting Statistics of Single Electron Transport in a Quantum Dot*, Phys. Rev. Lett. **96**, 076605 (2006).

[59] M. M. Desjardins et al., *Observation of the frozen charge of a Kondo resonance*, Nature **545**, 71 (2017).

[60] R Azouit, F Chittaro, A Sarlette, and P Rouchon. *Towards generic adiabatic elimination for bipartite open quantum systems*, Quantum Science and Technology, **2** 044011, (2017).

[61] P. Forni, A. Sarlette, T. Capelle, E. Flurin, S. Deléglise, and P. Rouchon, *Adiabatic elimination for multi-partite open quantum systems with non-trivial zero-order dynamics*, arXiv:1803.07810

[62] L. M. Sieberer, M. Buchhold, S. Diehl, *Keldysh Field Theory for Driven Open Quantum Systems*, Rep. Prog. Phys. **79**, 096001 (2016).

[63] Jean Zinn-Justin, Path Integrals in Quantum Mechanics, Oxford Graduate Texts, 2004.

[64] G. Gasse, C. Lupien, and B. Reulet, *Observation of Squeezing in the Electron Quantum Shot Noise of a Tunnel Junction*, Phys. Rev. Lett. **111**, 136601 (2013).

[65] J.-C. Forgues, C. Lupien, and B.Reulet, *Experimental Violation of Bell-like Inequalities By Electronic Shot Noise*, Phys. Rev. Lett. **114** 130403 (2015).

[66] U. C. Mendes and C. Mora, *Electron-photon interaction in a quantum point contact coupled to a microwave resonator*, Phys. Rev. B **93**, 235450 (2016).

[67] M. Westig et al. *Emission of non-classical radiation by inelastic Cooper pair tunneling*, Phys. Rev. Lett. **119**, 137001 (2017).

[68] A. L. Grimsmo, F. Qassemi, B. Reulet, and A. Blais, *Quantum Optics Theory of Electronic Noise in Coherent Conductors*, Phys. Rev. Lett. **116**, 043602 (2016).